

Francesco Zonta
Institute of Fluid Mechanics and
Heat Transfer,
Vienna University of Technology,
Getreidemarkt 9,
Vienna 1060, Austria
e-mail: francesco.zonta@tuwien.ac.at

Alfredo Soldati¹
Institute of Fluid Mechanics and
Heat Transfer,
Vienna University of Technology,
Getreidemarkt 9,
Vienna 1060, Austria;
DPIA,
University of Udine,
Udine 33100, Italy
e-mail: alfredo.soldati@tuwien.ac.at

Stably Stratified Wall-Bounded Turbulence

Stably stratified wall-bounded turbulence is commonly encountered in many industrial and environmental processes. The interaction between turbulence and stratification induces remarkable modifications on the entire flow field, which in turn influence the overall transfer rates of mass, momentum, and heat. Although a vast proportion of the parameter range of wall-bounded stably stratified turbulence is still unexplored (in particular when stratification is strong), numerical simulations and experiments have recently developed a fairly robust picture of the flow structure, also providing essential ground for addressing more complex problems of paramount technological, environmental and geophysical importance. In this paper, we review models used to describe the influence of stratification on turbulence, as well as numerical and experimental methods and flow configurations for studying the resulting dynamics. Conclusions with a view on current open issues will be also provided. [DOI: 10.1115/1.4040838]

1 Introduction

Turbulent stratified flows are a common occurrence in many industrial and natural processes. Industrial processes include cooling in nuclear reactors [1], fluid motion in heat transfer equipment [2,3], or fuel injection and combustion in gasoline engines [4]. Natural processes include the dynamics of the nocturnal atmospheric boundary layer [4,5], mixing in rivers and continental shelf seas [6], or the transport of organic species in the ocean [7].

The problem of stratified turbulence is quite complicated. Beyond the complexity of turbulence itself, we have to consider the presence of buoyancy forces that do depend on local density gradients. Fully specifying a turbulent stratified flow requires specifying many parameters, including the flow forcing and boundary conditions, the mean temperature gradient, and the fluid properties like density, viscosity, thermal conductivity, thermal expansion coefficient, and specific heat. Other factors that may be important include concentration and salinity gradients, rotational and multiphase flow effects, phase change, flow compressibility, and specific dependence of the fluid properties on the local temperature and pressure field. Critical applications often involve many of these complicating factors at once. For example, fuel injection and combustion in gasoline engines involves strong localized variations of fluid properties, flow compressibility, multiphase flow effects and phase change [4].

Stratified turbulence can be unbounded and homogeneous, as in the stratosphere or in the deep ocean [8–10]. However, stratified turbulence can be also unbounded and sheared, as for instance when the wind blows in the atmosphere or when deep currents stir the ocean [11–13], and finally, stratified turbulence can be bounded and sheared, as in the terrestrial and oceanic boundary layers [5,7,14] or in industrial applications [15]. But there is a simple and rich problem at the core of stably stratified turbulence: how do turbulent transport rates (of mass, momentum and heat) and mixing change for increasing stratification? When stratified turbulence is homogeneous, turbulence is not sustained by any applied shear and decays following an evolution in which buoyancy forces influence the largest flow scales first, and the smaller scales later, until the final turbulence collapse is reached [11]. When stratified turbulence is forced by an applied uniform shear, its dynamics is controlled by the gradient Richardson number

$Ri_g = N^2/S^2$, with S the value of the mean shear and N the Brunt–Väisälä frequency. Numerical and experimental results [16,17] indicate that if $Ri_g \simeq 0.25$, the turbulence neither grows nor decays. At lower values of Ri_g turbulence grows, whereas at higher ones it decays. Finally, when stratified turbulence is forced by an applied shear and at the same time influenced by the presence of a boundary, its evolution is not only controlled by the mean strength of shear and stratification, but also by their distributions as a function of the distance from the boundary [18].

In this review, we focus precisely on wall-bounded stratified turbulence. Many of the works in this field have considered Poiseuille flows in closed or open channels, consisting of long channels in which the flow is driven by a mean pressure gradient, and the stratification is imposed by prescribing a given density difference, $\Delta\rho = \rho_b - \rho_t$, between the bottom (ρ_b) and the top (ρ_t) boundary (alternatively, a negative density flux $d\rho/dz$ can be prescribed at the top boundary). The flow physics of such flows can be described in terms of three main parameters, namely the shear Reynolds number (Re_τ), the shear Richardson number (Ri_τ), and the Prandtl number (Pr)

$$Re_\tau = \frac{u_\tau h}{\nu_0}, \quad Ri_\tau = \frac{g\Delta\rho h}{\rho_0 u_\tau^2}, \quad Pr = \frac{\nu_0}{\kappa_0} \quad (1)$$

Quantities ρ_0 , ν_0 , and κ_0 are the reference fluid density, kinematic viscosity, and thermal diffusivity, and $u_\tau = (\tau_w/\rho_0)^{1/2}$ is the shear velocity (τ_w being the shear stress at the wall). The acceleration due to gravity is g , and h is the channel half-height. The density difference, $\Delta\rho$, can be either due to a temperature or a concentration difference. In this paper, we will mostly refer to the case of thermally stratified flow, which we consider an archetypal case also for density and concentration stratified flows, and for which the density difference can be written as $\Delta\rho/\rho_0 = -\beta_0\Delta T$, where β_0 is the reference thermal expansion coefficient and ΔT the top to bottom temperature difference. While the shear Reynolds number measures the competition between inertial and viscous forces, the shear Richardson number measures the competition between buoyancy and inertial forces, and the Prandtl number measures the momentum to thermal diffusivity ratio. Note that the reference temperature used to compute the fluid properties is usually the mean temperature between the top and bottom wall.

Wall-bounded stably stratified flows can be divided into two main categories, which are commonly referred to as the weakly/moderately and the strongly stratified case (or alternatively, weakly stable and very stable regimes [19]). In the weakly/moderately

¹Corresponding author.

Manuscript received March 16, 2018; final manuscript received July 10, 2018; published online August 9, 2018. Assoc. Editor: Jörg Schumacher.

stratified case, turbulence is actively sustained near the boundary, whereas intermittent turbulence, also flavored by the presence of nonturbulent wavy structures (internal gravity waves, IGW [20]), is observed at larger distances. In this case, an equilibrium regime is established between the production of turbulence by the mean shear and the suppression of turbulence by the stable stratification so that the Monin–Obukhov self-similarity theory [21,22] can be used. In the strongly stratified case, a global turbulent state cannot be sustained. As a result, the flow becomes intermittent, with regions characterized by complete turbulence suppressions, followed by regions in which turbulence is reactivated. Note, however, that the classification of stably stratified wall bounded flows into these two main categories is only a pedagogical simplification that will help us organizing the literature material we wish to present.

To provide a concrete example of the rich dynamics arising from the mutual interaction between buoyancy and turbulence in wall-bounded flows, we examine an instantaneous flow field. With the aid of direct numerical simulations (DNSs), the temperature contours were measured and rendered in a perspective three-dimensional view (Fig. 1). Based on the behavior of these temperature contours, we identify two main flow regions. First, there is a region close to the boundary where the flow behaves like a classical turbulent boundary layer. In this region, the mean shear produces turbulent kinetic energy and generates small-scale vorticity that is almost insensitive to the flow stratification. Farther from the wall, where vortices and flow structures are larger, stratification becomes important, and the flow differs from the one observed in the near wall region. At these distances from the wall we notice the appearance of IGW. The origin of IGW is intimately related to the behavior of the density profile as a function of the distance z from the bottom boundary. If density decreases for increasing z , a fluid particle that is displaced vertically by velocity fluctuations is subject to a buoyancy force that tends to bring it back to its initial position. The fluid particle can overshoot inertially and oscillate, generating a wavy motion.

Naturally, IGWs interact with the turbulent flow field and dramatically alter mixing and vertical transfer rates [15,23], which are now characterized by several characteristic lengthscales. Such characteristics lengthscales are produced by the interplay between inertial forces (induced by the applied shear or pressure gradient) and buoyancy forces (induced by the stable stratification). In wall-bounded flows, inertial and buoyancy forces are not homogeneous and change steeply moving away from the wall, making their ratio dependent on the distance from the wall. A precise local measure of the relative importance of these two competing forces can be assessed by comparing the corresponding length scales. Buoyancy forces act preferentially on the large scales of vertical motion,

creating an upper bound for the vertical size of turbulent eddies. An estimate of the smallest scale influenced by buoyancy is given by the Ozmidov scale (obtained by Ozmidov [24] from an order of magnitude analysis between buoyancy and inertial forces, see also Refs. [25] and [26])

$$L_o = \left(\frac{\varepsilon}{N^3} \right)^{1/2} \quad (2)$$

in which ε is the turbulent kinetic energy dissipation rate, and N is the Brunt–Väisälä frequency (which will be characterized below). Sometimes the Thorpe scale L_t , based on the estimate of density inversions of an instantaneous density profile, is used in place of the Ozmidov scale L_o to evaluate the scale at which buoyancy influences turbulent motions [11,27–30]. This is usually done in large-scale experiments (see for instance Ref. [31]) where the instantaneous density profile is more easily accessible compared to ε , which indeed requires the knowledge of the distribution of small-scale velocity derivatives. Again, in addition to the Ozmidov scale, the Monin–Obukhov length scale L_{MO} [21,22,32] is often preferred to estimate the distance from a boundary at which turbulence generation by shear and by buoyancy are of the same order (i.e., the distance at which buoyancy starts influencing the dynamics). The Monin–Obukhov length scale L_{MO} is defined as

$$L_{MO} = \frac{\rho_0 u_\tau^3}{C_k g q_w} \quad (3)$$

where $C_k \simeq 0.4$ is the Von Kármán constant, and q_w is the wall heat flux.

Differently from buoyancy, turbulence is characterized by a broad range of spatial scales. At one extreme of the scale domain, we have the Kolmogorov length scale [33]

$$\eta = \left(\frac{\nu_0^3}{\varepsilon} \right)^{1/4} \quad (4)$$

which is the smallest flow scale that can be observed in a turbulent environment without being dissipated into heat by viscosity. At the opposite extreme of the scale range we have the largest turbulent scales, whose size can be estimated via the Ellison scale [30,31,34]

$$L_e = \left(\frac{\langle \rho^2 \rangle^{1/2}}{\partial \langle \rho \rangle / \partial z} \right)^{1/4} \quad (5)$$

that makes use of the density fluctuations as a marker of turbulent motions. An alternative choice, perhaps more related to the physics of wall-bounded flows is the use of the distance to the nearest boundary, L_z , as the local measure of the largest scale of turbulence at a given location [35]. Figure 2 shows the behavior of the different scales, L_o/h , $9\eta/h$, and L_e/h in a stratified turbulent channel from the boundary ($z/h=0$) up to the channel center ($z/h=1$) and corresponding to the lower half of the domain rendered in Fig. 1. A similar distribution of scales can be observed in open channel flows, possibly assuming different boundary conditions [6,35]. Note that 9η is used instead of η alone following Itswire et al. [30], who argued that a buoyancy-controlled scenario is established when $L_o \simeq 9\eta$. A pictorial view of the flow structure using vectors (the length of which indicates their magnitude) is also shown in Fig. 2(a). From the behavior of the relevant flow scales, three main regions can be identified [11,30,35]. In proximity of the wall, where the values of shear are higher, L_o is larger than the characteristic local flow scales, and the flow is controlled by turbulence. In this region (*turbulence dominated region*), the departure of the flow from unstratified conditions is expected to be very small. At larger distances from the wall, the values of shear decrease and so does L_o , while both the smallest and the

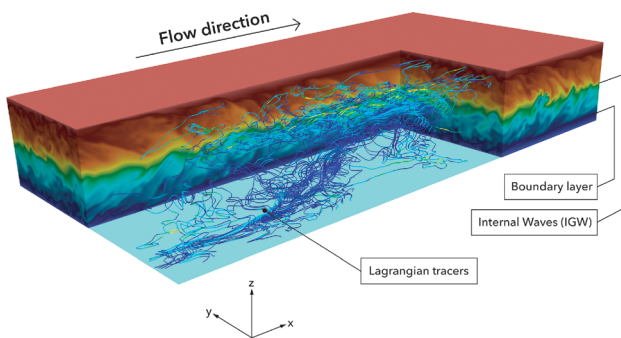


Fig. 1 The structure of a weakly/moderately stratified wall-bounded turbulent flow. Close to the boundary, classical boundary layer turbulence is sustained. Farther from the wall, a buoyancy dominated region characterized by the presence of IGWs is observed. Contour maps of the temperature field are used for visualization purposes. Trajectories of Lagrangian tracers randomly released in the flow and colored by the magnitude of their turbulent kinetic energy are also shown. The flow direction is explicitly indicated.

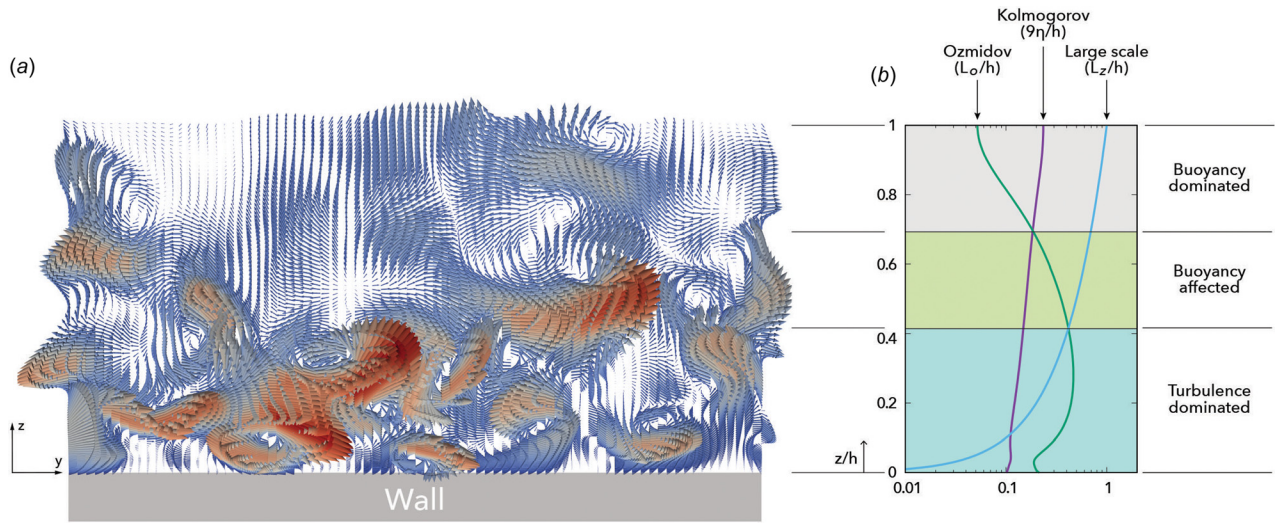


Fig. 2 Panel (a) vector plots on a y - z cross section of a stratified channel (only half of the channel, from the boundary up to the channel center, is shown); (b) Wall-normal behavior of the Ozmidov scale (L_o/h), Kolmogorov scale ($9\eta/h$), and distance from the boundary (L_z/h , taken here as representative for the largest turbulence scales). Results from Ref. [36].

largest scales of turbulence increase. As a result, buoyancy influences the largest flow scales first (in the *buoyancy-affected region*), the smallest flow scales later (in the *buoyancy-dominated region*). The extension of the different regions is qualitatively sketched in Fig. 2(b).

This paper reviews the status of our understanding of the complex interaction between wall-bounded turbulence and stratification. We focus mainly on the foundational problem that can be rigorously addressed using the Oberbeck–Boussinesq (OB) [37,38] approximation. Extension to more complex cases, including the behavior of stratified turbulence under non-Oberbeck–Boussinesq (NOB) conditions are also discussed. We organize the paper as follows: Sec. 2 reviews mathematical models that describe the dynamics of turbulence in a stratified environment. We introduce the Oberbeck–Boussinesq approximation and we discuss its range of validity. We examine methods and flow configurations used in numerical simulations in Sec. 3 and those used in experiments in Sec. 4. In Sec. 5, we discuss the flow structure and the general features of wall-bounded stratified flows for both weakly and strongly stratified cases. In Sec. 6, we consider the effect of stratification on heat and momentum transfer rates (Nusselt number and friction factor) in wall-bounded turbulence. In Sec. 7, we will go beyond the common Oberbeck–Boussinesq approximation discussing the effects of flow compressibility and nonuniform fluid properties on the overall dynamics of the flow. Finally, in Secs. 8 and 9, we will draw conclusions and outline possible fields of future research. In the context of this paper, in which we examine only the case of stably stratified turbulence, we will drop the word stably for ease of reading hereinafter.

2 Equations of Motion for Wall-Bounded Stratified Flows

The full nonlinear continuity, momentum, and energy equations describing the motion of a compressible stratified flow represent a complex system of coupled equations that is in general difficult to solve. In many cases, the complete set of the governing equations can be conveniently simplified by introducing the Oberbeck–Boussinesq (OB) approximation. In this section, we introduce the general compressible form of the governing equations (NOB) first, the OB approximation later. A discussion on the ranges of validity of the OB approximation is also provided.

2.1 General Form of the Governing Equations. The most general starting point for the analysis of stably stratified

turbulence is represented by the complete system of continuity, momentum, and energy equations for a Newtonian fluid of variable properties and second viscosity equal to zero [39]

$$\frac{D\rho}{Dt} + \rho \frac{\partial u_i}{\partial x_i} = 0 \quad (6)$$

$$\rho \frac{Du_i}{Dt} = -\frac{\partial P}{\partial x_i} - \rho g \delta_{3,i} + \mu \frac{\partial \Gamma_{ij}}{\partial x_j} + \Gamma_{ij} \frac{\partial \mu}{\partial x_j} \quad (7)$$

$$\rho c_p \frac{DT}{Dt} = \lambda \frac{\partial^2 T}{\partial x_j^2} + \frac{\partial \lambda}{\partial x_j} \frac{\partial T}{\partial x_j} + \beta T \frac{DP}{Dt} + \mu \Phi \quad (8)$$

where u_i are the fluid velocity components, P is the pressure, and T is the temperature. Note that

$$\Gamma_{ij} = \frac{\partial u_i}{\partial x_j} + \frac{\partial u_j}{\partial x_i} - \frac{2}{3} \frac{\partial u_k}{\partial x_k} \delta_{ij}, \quad \Phi = \frac{1}{2} \Gamma_{ij} \left(\frac{\partial u_i}{\partial x_j} + \frac{\partial u_j}{\partial x_i} \right) \quad (9)$$

are the rate of strain tensor (Γ_{ij}) and the rate of dissipation of mechanical energy due to viscosity (Φ), whereas the thermophysical fluid properties are density ρ , viscosity μ , specific heat c_p , and thermal expansion coefficient $\beta = -1/\rho(\partial\rho/\partial T)_p$. To fully specify the problem, suitable laws for the determination of the fluid properties as a function of temperature and pressure must be prescribed. These can be given in the general form

$$\begin{aligned} \rho &= \rho(T, P), & c_p &= c_p(T, P) \\ \mu &= \mu(T, P), & \beta &= \beta(T, P), & \lambda &= \lambda(T, P) \end{aligned} \quad (10)$$

In most cases, such laws are inferred from the available analytical expressions and correlations derived from thermodynamics and/or experimental measurements [36,40–43]. Equations (6)–(8), complemented with explicit laws to particularize Eq. (10), constitute the general form of the governing equations. In connection with Sec. 2.2, and precisely to stress the difference with the commonly adopted OB approximation, this form is usually called NOB.

2.2 Oberbeck–Boussinesq Approximation. The OB approximation [37,38] is based on the assumption that fluid density variations are small enough to be negligible in the continuity equation and play a role only in the gravitational term of the momentum equation (i.e., where ρ is multiplied by the

acceleration due to gravity g). The reason why is it possible to assume a constant ρ but in the gravitational term, is that the product ρg can produce large effects even when relative density fluctuations with respect to the reference density ρ_0 are very small (i.e., $(\rho - \rho_0)/\rho_0 \ll 1$), since acceleration due to gravity is in general much larger than any other local value of the fluid acceleration (i.e., $|g| \gg |Du_i/Dt|$). Further, in the OB approximation all thermophysical fluid properties are strictly constant and uniform. Then, governing equations can be conveniently written in dimensionless form. Without the loss of generality, we refer to the case of a density-stratified Poiseuille flow in a closed channel, in which the stable stratification is maintained by keeping a positive density difference $\Delta\rho = \rho_b - \rho_t$ between the bottom (ρ_b) and the top (ρ_t) walls. The OB form of the governing balance equations reads as

$$\frac{\partial u_i}{\partial x_i} = 0 \quad (11)$$

$$\frac{Du_i}{Dt} = -\frac{\partial p'}{\partial x_i} + \frac{1}{\text{Re}_\tau} \frac{\partial^2 u_i}{\partial x_j^2} - \text{Ri}_\tau \rho' \delta_{3,i} + \delta_{1,i} \quad (12)$$

$$\frac{D\rho}{Dt} = \frac{1}{\text{Re}_\tau \text{Pr}} \frac{\partial^2 \rho}{\partial x_j^2} \quad (13)$$

where in this case p' represents the pressure deviation from the hydrostatic reference case, ρ' is the density fluctuation, and $\delta_{1,i}$ is the mean pressure gradient driving the flow. The three parameters appearing in Eqs. (11)–(13) are the shear Reynolds number Re_τ , the shear Richardson number Ri_τ , and the Prandtl number Pr already defined above (see Sec. 1).

Alternative definitions of the Richardson number are used in the literature to describe and parameterize the dynamics of stratified turbulence. The different definitions of the Richardson numbers are based on different definitions of the reference velocity scale used to write equations in dimensionless form. Therefore, we have the centerline Richardson number (which takes the centerline velocity u_c as reference), the bulk Richardson number Ri_b (which takes the bulk velocity u_b as reference), and the gradient Richardson number $\text{Ri}_g = N^2/S^2$ (which takes the Brunt Vaisala frequency N and the mean shear rate S as reference parameters). Although Ri_τ is customarily used for the characterization of the flow regimes in numerical simulations of wall-bounded stratified flows [18,36,44,45], its use in experiments is much more limited. Reasons are related to the difficulty in the determination of the shear velocity u_τ (that in turn requires the determination of the wall shear stress). Therefore, in experiments the bulk Richardson number Ri_b is usually preferred, since the bulk velocity is an easier quantity to access.

2.3 Range of Validity of the Oberbeck–Boussinesq Approximation. A number of important aspects of the flow physics in the broad field of buoyancy-influenced flows [46–48] was elucidated by employing the OB approximation (Eqs. (11)–(13)). It should be remarked here, however, that it represents a good approximation of the exact equations (Eqs. (6)–(8)) within certain ranges of variation of the main parameters only [49–53], and its applicability beyond these ranges is not physically justified. To understand it, we estimate the accuracy error introduced by the assumption of constant density in the continuity equation by computing the ratio between the material derivative of density $\rho^{-1}D\rho/Dt$ and the divergence of the velocity field $\partial u_j/\partial x_j$ [54,55]. Upon introduction of appropriate length (l_0), velocity (u_0), and temperature (ΔT) scales, we get

$$\frac{\rho^{-1}D\rho/Dt}{\partial u_j/\partial x_j} = \frac{\beta DT/Dt}{\partial u_j/\partial x_j} \simeq \frac{\beta \Delta T (u_0/l_0)}{u_0/l_0} = \beta \Delta T \quad (14)$$

To derive Eq. (14), u_0 is considered small compared to the speed of sound c (i.e., the Mach number $\text{Ma} = u_0/c < 0.3$) and pressure

changes in the fluid are considered slow compared to acoustic pressure waves. Therefore, for the OB approximation to be valid, $\beta \Delta T \ll 1$. However, this represents only a rough estimate. Precise boundaries for the validity of the OB approximation were obtained by Gray and Giorgini [51] starting from the full nonlinear equations in compressible form and writing all the fluid properties as a linear Taylor expansion of temperature and pressure, i.e.,

$$\begin{aligned} \rho &= \rho_0[1 - \beta_0(T - T_0) + \gamma_0(P - P_0)] \\ c_p &= c_{p0}[1 - a_0(T - T_0) + b_0(P - P_0)] \\ \mu &= \mu_0[1 - c_0(T - T_0) + d_0(P - P_0)] \\ \beta &= \beta_0[1 - e_0(T - T_0) + f_0(P - P_0)] \\ \lambda &= \lambda_0[1 - m_0(T - T_0) + n_0(P - P_0)] \end{aligned}$$

After retaining only the leading order terms of the resulting equations, Gray and Giorgini [51] were able to derive a set of constraints for the OB approximation to be valid. These constraints were written in the following form:

$$\begin{aligned} \varepsilon_1 &= \beta_0 \Delta T \leq \delta, & \varepsilon_2 &= \gamma_0 \rho_0 g h \leq \delta \\ \varepsilon_3 &= c_0 \Delta T \leq \delta, & \varepsilon_4 &= d_0 \rho_0 g h \leq \delta \\ \varepsilon_5 &= a_0 \rho_0 g h \leq \delta, & \varepsilon_6 &= b_0 \rho_0 g h \leq \delta \\ \varepsilon_7 &= m_0 \Delta T \leq \delta, & \varepsilon_8 &= n_0 \rho_0 g h \leq \delta \\ \varepsilon_9 &= e_0 \Delta T \leq \delta, & \varepsilon_{10} &= f_0 \rho_0 g h \leq \delta \\ \varepsilon_{11} &= \beta_0 g h / c p_0 \leq \delta \\ \varepsilon_{12} &= \varepsilon_{11} T_0 / \Delta T \leq \delta \end{aligned}$$

where $\delta = 0.1$ is a small enough number (i.e., giving a maximum error of 10% in the estimate of the fluid property). That is to say, when $\delta \leq 0.1$, the value of each fluid property can be safely approximated by its reference value (indicated by the subscript 0). A further restrictive condition, i.e., $\varepsilon_{12} < 0.02$, for the work done by pressure forces and the heat generated by viscous losses to be negligible, has been recently proposed by Pons and Quéré [56]. Altogether, these constraints set the boundaries for an explicit evaluation of the validity ranges of the OB approximation. These are plotted in Fig. 3 for the case of air (Fig. 3(a)) and water (Fig. 3(b)) at reference temperature $T_0 = 15^\circ\text{C}$ and pressure $P_0 = 10^5$ Pa. The two main parameters are the temperature difference ΔT and the characteristic size of the problem h . The values of the thermophysical properties at the reference conditions are evaluated as in Ref. [51]. For air, the most restrictive conditions are ε_1 (variation of ρ with T), ε_2 (variation of ρ with P), and ε_{12} (pressure work term). For water, the most restrictive conditions are ε_9 (variation of β with T), ε_8 (variation of λ with P), and ε_{12} (pressure work term). Sometimes, when liquids are used as working fluids at a reference temperature different from the commonly adopted $T_0 = 15^\circ\text{C}$, ε_2 (variation of μ with temperature) can become as important as ε_9 (see for instance Zonta et al. [36,43]) in determining the proper thresholds for the validity of the OB approximation.

The widely used OB approximation is physically sound in the area labelled Oberbeck–Boussinesq approximation of Fig. 3 only. The extended Boussinesq model (sometimes called thermodynamic Boussinesq model, see Ref. [56]) accounting for the pressure-work term in the energy equation has a validity that includes also the region labelled Thermodynamic Boussinesq in Fig. 3. Outside these ranges, NOB approaches must be used. While the low-Mach number approximation (also known as an elastic approximation [57–59], see the corresponding regions in Fig. 3) are required for air flows (since the most restrictive condition is the dependence of ρ on T and P), alternative solutions accounting for the temperature or pressure variation of μ , β or λ [36,60,61] are adequate for water (and other liquid) flows in many situations far from critical points (regions labelled Incompressible non-Oberbeck–Boussinesq in Fig. 3). The case of liquid flows close to critical conditions must be analyzed with a low-Mach number approximation as well [40–42].

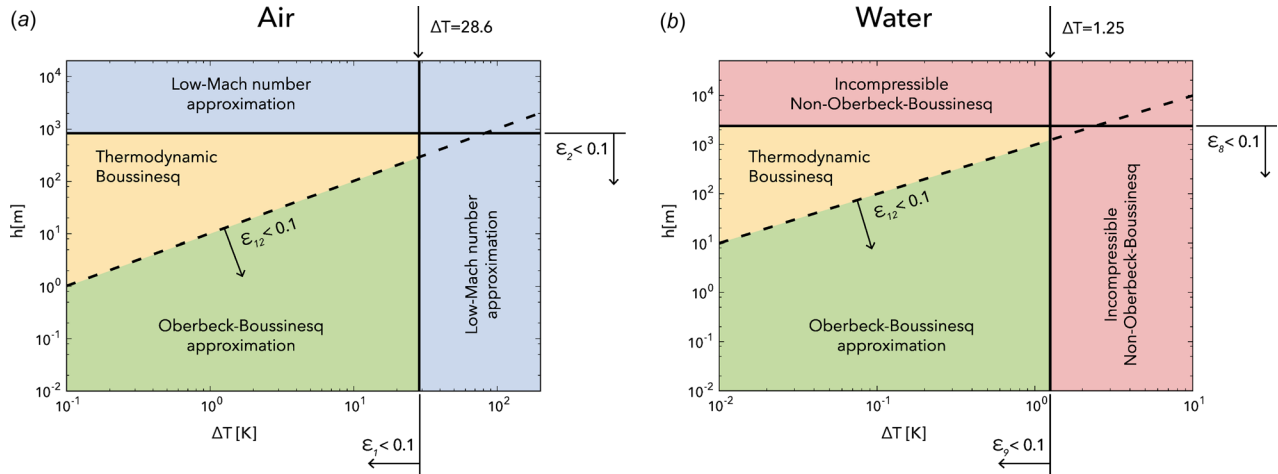


Fig. 3 A parameter space (ΔT , h) of wall-bounded stratified turbulence with the different numerical approach that can be used for its description. Panel (a): air; panel (b): water. In this schematic, the solid lines indicate approximately the point at which the basic Oberbeck–Boussinesq model begins to fail, and more complex non-Oberbeck–Boussinesq models (both incompressible NOB or low-Mach) must be used. The dashed line indicates the point at which the thermodynamic Boussinesq model should be used. Specific indication of the parameter (ϵ) that describes each threshold line is also explicitly given. The label inside each region indicates the corresponding numerical approach according to the following color-code: Oberbeck–Boussinesq, low-Mach number, incompressible NOB, and thermodynamic Boussinesq. Some examples of the most suitable approaches to be used for flows of interest in environmental and industrial applications are provided in the following. In the nocturnal boundary layer, for example, $h \approx 10^2/10^3$ m and $\Delta T \approx 5$ °C. In this case, the thermodynamic Boussinesq model would be appropriate. However, if $h > 10^3$ m, a low-Mach number approach would be recommended. In the deep ocean, $h \approx 10^3$ m and $\Delta T \approx 2$ °C, whereas in the upper ocean, $h \approx 10^2$ m and $\Delta T \approx 10$ °C [62]. In both cases, an incompressible NOB approach is required. In industrial heat transfer processes, typical sizes are $h \approx 1$ m, whereas ΔT are usually larger than in environmental applications. For air, temperature gradients can easily be $\Delta T = 10/100$ °C, while for water ΔT can achieve few tens, in particular for high heat flux cooling technologies [63]. In these latter cases, a low Mach number approach (air) and an incompressible NOB approach (water) is recommended.

3 Computational Approaches

The available approaches to compute turbulent flows are DNS, large eddy simulation (LES), and Reynolds-averaged Navier–Stokes (RANS). We refer the reader to already existing archival reviews [64–66] for further details on these topics. Here, we will limit our discussion to the application of each of these approaches to stratified turbulence. However, instrumental to elucidate some features of this type of flows, we dedicate the first paragraph of this section to the stability analysis of a stratified channel.

3.1 Linear Stability Analysis of Wall-Bounded Stratified Flow. A plane Poiseuille flow subject to an external stabilizing density/temperature gradient and characterized by a given Reynolds number Re is asymptotically stable if the Richardson number exceeds a critical value Ri_{cr} (which in general depends on the value of Re). In 1961, Miles [67] developed a stability theory for stratified flows based on the inviscid flow equations. Few years later, Gage and Reid [68] extended the theory of Miles using the complete set of Navier–Stokes equations. In their stability analysis of a stratified laminar Poiseuille flow, Gage and Reid [68] identified the dependence of the critical Richardson number Ri_{cr} on Re . As usual in laminar Poiseuille flows, they used the centerline velocity as a reference scale and adopted the critical centerline Richardson number $Ri_{c,cr} = g\beta h\Delta T / (8u_c^2)$, as well as the centerline Reynolds number $Re_c = u_c h / \nu$, as the main parameters. Note that here the Richardson number is defined based on the temperature difference rather than on the density difference, i.e., $\Delta\rho / \rho_0 = \beta\Delta T$. More recently, Armenio and Sarkar [18] recast the stability threshold found by Gage and Reid [68] in terms of the shear Richardson number defined as

$$Ri_{\tau,cr} = 8Ri_{c,cr} \frac{Re_c^2}{Re_\tau^2} \quad (15)$$

Considering that the velocity profile in a laminar Poiseuille flow is parabolic and its derivative at the wall is $du/dz|_w = u_c^2/\nu = 2u_c/h$, they obtained $Re_c = Re_\tau^2/2$ and finally got

$$Ri_{\tau,cr} = 2Ri_{c,cr}Re_\tau^2 \quad (16)$$

Equation 16 combined with the results of Gage and Reid [68], can be used to draw the black circles (\bullet) in the (Re_τ , Ri_τ) phase diagram shown in Fig. 4. With a black solid line, we plot what we propose here as a best-fit explicit relationship $Ri_\tau = f(Re_\tau)$ (the detailed best-fit expression is reported in the figure). Also shown (symbols) in Fig. 4 are the results of different campaigns of numerical simulations [6,36,45,69–71]. Based on the results shown in Fig. 4, the presence of three different regimes can be observed [18,30,44,45]: a weakly stratified turbulent regime, a strongly stratified turbulent regime, and a strongly stratified laminar regime. The lower boundary at which the strongly stratified turbulent regime begins (shaded area) is heuristically drawn based on the results of numerical simulations and is intended here for conceptual use only. In the weakly stratified turbulent regime, turbulence is modified only far from the wall, with the near wall region maintaining the classical structure of unstratified turbulence. In the strongly stratified turbulent regime (shaded area in Fig. 4), stratification influences also the near wall region, which becomes populated by laminar patches, although the mean flow is still able to sustain turbulence. Increasing further the stratification level and trespassing the threshold represented by the neutral stability curve (behavior of $Ri_{\tau,cr}$, solid line), turbulence is completely suppressed by buoyancy, and the flow is fully laminar [68]. Based on the value of the shear Richardson number Ri_τ , the concept of subcritical (i.e., characterized by small-than-critical value of Ri_τ) or supercritical (i.e., characterized by larger-than-critical value of Ri_τ) conditions is usually introduced [18].

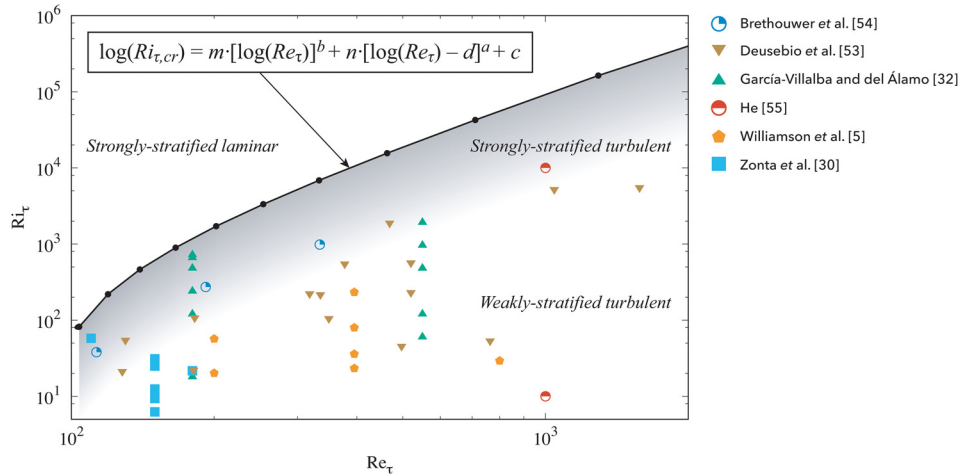


Fig. 4 Structure of the $(Re_\tau - Ri_\tau)$ space diagram for wall bounded stratified flows. Circles represent the critical Ri_τ (neutral curve) obtained from the linear stability analysis [68] and recast to fit with the present parameter space. The fitting of the neutral curve proposed here has the following form: $\log(Ri_{\tau,cr}) = m \cdot [\log(Re_\tau)]^b + n \cdot [\log(Re_\tau) - d]^a + c$, where the value of the parameters is $a = -0.1843$, $b = 1.047$, $c = 1.914$, $d = 1.927$, $m = 1.651$, and $n = -2.204$. The shaded area in the parameter space corresponds to strongly stratified turbulent flow conditions (appearance of laminar patches in the near wall region). The strongly stratified laminar and the weakly stratified turbulent regions are also explicitly indicated. Symbols below the neutral curve represent a collection of numerical simulations of wall-bounded stratified turbulence [6,36,45,69–71]. Note that, in the context of stably stratified turbulence, the term subcritical (resp. supercritical) condition refers to a flow characterized by a lower-than-critical (resp. larger-than-critical) value of the shear Richardson number Ri_τ , i.e., falling below (resp. above) the neutral curve.

There is still a bit of uncertainty about the complete relaminarization of strongly stratified flows. Building on the works of Nieuwstadt [14] and Der Wiel et al. [72], Donda et al. [73] have recently argued that the laminarization process induced by stratification is an inherently transient phenomenon, which is always followed by a recovery of turbulence provided that sufficiently large finite amplitude perturbation are imposed on the laminarized state and provided that sufficient time for flow acceleration is allowed.

3.2 Direct Numerical Simulation. Direct numerical simulation discretize the governing equations on a spatio-temporal grid fine enough to resolve all the scales of the turbulent motion down to the smallest, which is represented by the Kolmogorov scale η (already defined above) for $Pr < 1$ or by the Batchelor scale $\eta_B = \eta/Pr$ for $Pr > 1$ [33,74]. In unstratified wall-bounded turbulence, vertical scales are usually smaller (but of the same order of magnitude) than horizontal scales. In stratified wall-bounded turbulence, the scale separation becomes larger, with the vertical scales being usually orders of magnitude smaller than the horizontal scales. This poses further constraints on the computational cost of each simulation.

Since DNS computes turbulence without the aid of any model, it has the unique capability to capture all the flow details and to quantify all terms in the fundamental energy and momentum budgets, even those that cannot be experimentally measured. This is of specific importance for strongly stratified flows, where vigorous local turbulence events and sharp gradients of temperature and/or of material properties may lead to strong, spatially and temporally localized mixing and transport that may be remarkably different from the mean turbulence statistics. Many DNS studies of wall-bounded stratified turbulence have been performed in closed or open plane channels and using different computational techniques. While simulations run in closed channels aim at mimicking internal flows of interest for industrial applications [36,45,75,76], simulations in open channels and boundary layers [6,14,70,71,75–81] are mostly motivated by environmental and geophysical applications (terrestrial and oceanic boundary layers). Despite some differences that may arise from the specific

boundary conditions adopted, stratification in open channels and boundary layers is similar to that observed in closed channels.

Direct numerical simulation of stably stratified channel turbulence was first performed by Iida et al. [75] for weakly/moderately stratified conditions in a closed channel at shear Reynolds number $Re_\tau = 150$, and by Nieuwstadt [14] for strongly stratified conditions in an open channel flow at shear Reynolds number $Re_\tau = 395$. Few years later, the DNS studies of Flores and Riley [77] and García-Villalba and del Álamo [45] have largely contributed to the physical comprehension of the dynamics of wall-bounded stratified turbulence. One of the crucial aspects raised by these DNS studies was the need of very large domains to properly characterize the turbulent structures present in stratified channels. This is of specific importance for strongly stratified conditions, in which stratification effects fall well into the near-wall region inducing localized relaminarization patterns and a corresponding flow intermittency (see Sec. 5.2 for further details). The parameter range was further widened by subsequent works, increasing both the Reynolds and the Richardson numbers [6,69,70] so to explore weakly and strongly stratified conditions at values of Re_τ and Ri_τ progressively closer to those characterizing real applications. Recently, He [71] has performed DNS of an open channel flow at the unprecedented values of the Reynolds number $Re_\tau = 10^5$ and Richardson number $Ri_\tau = 10^4$ (a combination leading to a bulk Reynolds number of the order of $Re = 10^5$), obtaining intriguing results on the phenomenon of global intermittency in the strongly stable regime.

Even though it is not the primary object of this review, it is important to mention a number of studies which analyzed unbounded, yet sheared, stratified turbulence [11–13,82,83]. More recently, DNS has become the preferred tool to investigate NOB effects. These effects, usually arising when the flow is subject to strong thermal gradients [36,40,42] will be discussed more in detail in Sec. 7.

3.3 Large Eddy Simulation. In LES, only the largest scales are resolved by the computational grid and directly simulated, while the effects of the flow scales falling below the grid

resolution are parameterized by an appropriate subgrid-scale (SGS) model. Since its appearance, LES has been widely used in the analysis of stratified wall-bounded turbulence due to the lower computational cost required to perform such simulations at values of the governing parameters that are already of practical interest.

Motivated by the important geophysical and environmental applications (mainly atmospheric boundary layer), LES has been originally applied to study stratified boundary layers. Building on a heterogeneous database of available models [84–86] and field measurements [87], Mason and Derbyshire [88] and Derbyshire [89] showed the reliability of standard LES simulations run with a standard Smagorinsky SGS model to capture the dynamics and the main statistics of a weakly stratified boundary layer. Follow up studies to this work improved the SGS model using an additional transport equation for the subgrid kinetic energy [90], possibly combined with a nonlinear eddy diffusivity model [91]. A further improvement in the simulation of stratified boundary layers was achieved by Beare et al. [92] and Kleissl et al. [93] with the adoption of the dynamic model first introduced by Germano et al. [94]. Relaxing the main assumptions of the dynamic model (the model coefficient are scale independent and only slightly changing in space), Porté-Agel and coworkers [95,96] developed a scale-dependent Lagrangian model with appealing features for the analysis of atmospheric boundary layers. In most LES of geophysical and environmental situations, the near-wall region is not resolved and some kind of wall models is used.

Considering the case of stratified turbulent channels, the first systematic studies paving the way for future research in the field were those of Garg et al. [44] and Armenio and Sarkar [18], which performed wall-resolved LES of a turbulent flow at a given shear Reynolds number $Re_\tau = 180$ and for a wide range of stratification levels. Unlike in previous investigations, the shear Richardson number Ri_τ was found to characterize properly the dynamics of stratified turbulence. These studies were later extended considering different boundary conditions (free surface flows with a prescribed density flux [35]) and widening the range of the governing parameters (oscillating boundary layer, larger Prandtl number [97]).

One important aspect to be mentioned is that, while LES is suited for weakly and moderately stratified flows [90–92], its application to strongly stratified conditions is much more problematic [77]. A comprehensive discussion on the range of applicability of the standard LES models to wall-bounded stratified flows was proposed by Jiménez and Cuxart [98], who benchmarked the results of a large campaign of LES against a series of reliable and carefully realized field measurements (SABLES-98, [99] and CASES-99, [100], discussed in Sec. 4.2), and noticed that standard LES models work fairly well for weakly and for a short range of moderately stratified conditions. But they fall short of predicting strongly stratified conditions. The reason of this failure is twofold: first, the reduction of size of the characteristic structures is more demanding for the subgrid scale modeling (and the assumption of an isotropic and universal behavior questionable); second, strongly stratified turbulence is intermittent and localized in space, a situation that is hard to handle by LES models with horizontal averaging [96].

3.4 Reynolds-Averaged Navier–Stokes Equations. Direct numerical simulation and LES are too expensive for most practical flow problems and therefore only suitable to very idealized flows [33]. In such cases, the RANS approach is used. This approach, which is based on averaging the governing equations using the Reynolds decomposition, generates additional terms (usually referred to as Reynolds stresses) that account for turbulent momentum and heat transfer rates. Due to the appearance of terms containing fluctuations of the main variables, the number of unknowns is larger than the number of equations (that describe the evolution of the mean quantities only). The resulting problem cannot be solved in this form, and specific closure techniques are

therefore required. The simplest and widely used closure approach relies on the gradient diffusion hypothesis (first order closure), for which the turbulent momentum and heat fluxes are transported down the gradient of velocity and temperature, respectively. Within this approach, the closure problem reduces to the determination of the two coefficients of proportionality between the turbulent fluxes and the mean gradients of momentum and heat. These coefficients are usually referred to as eddy viscosity, ν_t , and eddy diffusivity, κ_t , respectively. Common approaches to estimate ν_t and κ_t go from simple algebraic models to more complex two-equation models [101]. The turbulent Prandtl number, $Pr_t = \nu_t/\kappa_t$, is often introduced to relate the turbulent momentum and heat fluxes.

In wall-bounded stratified flows, Pr_t is in general influenced by the density stratification and by the presence of the wall, although the latter is sometimes neglected [102–104]. When the presence of the wall is taken into account, one popular parameterization scheme invokes the Monin–Obukhov similarity theory [105] to model the effects of stratification on eddy diffusivities, possibly complemented by a correction function that does depend on the value of Ri_g . While this approach generally yields good results for weakly stable conditions [106], it introduces a threshold value for the gradient Richardson number $Ri_g = 0.2$, beyond which turbulent mixing is totally suppressed [107,108]. This does not agree with observations [109,110] and numerical simulations [91,111] which show that turbulent mixing persists for values of Ri_g well above $Ri_g = 0.2$. To solve this shortcoming, Huang et al. [107] have proposed a novel mixing-length model that still employs Ri_g to characterize stability, but does not introduce the correction function and does not invoke a critical Ri_g . This model agrees much better with LES results and converges to the classic model under neutral conditions. A simple, yet reliable model for Pr_t accounting for the flow inhomogeneity due to the presence of the wall has been recently introduced by Karimpour and Venayagamoorthy [112]. The model, which introduces a linear correction to Pr_t with the distance from the wall, has been benchmarked against available DNS databases [45] with satisfactory results.

More complex higher-order closure models, such as the Mellor–Yamada [113] and further declinations, have been also developed and tested for prediction of wall-bounded stratified turbulence. One of the main challenges associated with these higher-order methods is the introduction of further equations adding empirical constants that must be determined. Further, higher-order closure models usually foresee the presence of a maximum gradient Richardson number Ri_g above which the flow is completely laminar, and hence, encounter the very same limitations discussed above. Extensions to overcome these limitations have been recently proposed [114,115] and successfully applied. In particular, Lazeroms et al. [115] have derived an explicit algebraic model having the property of being general (independence on the adopted reference system), accurate and yet simple, since the nonlinear part of the Reynolds stresses and heat transport equations have been retained and solved in an approximate fashion. Such model has shown good agreement with DNS data for different kind of flows [45,69]. We remark that RANS models hardly predict the behavior of strongly stratified flows characterized by strong intermittency and spatial inhomogeneity as well [77]. Further complications arise when the flow is characterized by a sharp variation of the fluid properties [116].

4 Experimental Investigations

Wall-bounded stratified turbulence has been the object of a number of experimental investigations. Here, we will review both laboratory experiments and field measurements, listing the most important techniques and describing the main findings.

4.1 Laboratory Experiments. Laboratory experiments and field measurements of turbulence quantities in wall-bounded stratified turbulence are relatively scarce compared to the

unbounded case [16,117], primarily because of inherent difficulties in performing measurements close to a boundary.

One of the first experimental study to characterize the dynamics of wall-bounded stratified turbulence was done by Arya [118]. By considering a stratified boundary layer of air developing over a cooled/heated wall, Arya [118] found that stable stratification alters the mean velocity and temperature profiles and reduces the turbulence intensities, friction factor, and Nusselt number. Few years later, Komori et al. [119] studied the stratified flow obtained by condensing steam over the upper surface of an open channel and found similar results. One important observation made by Komori et al. [119] was that, for large stratification values, wave-like structures associated with counter gradient heat and momentum fluxes were observed. The gradient Richardson Ri_g was chosen as the indicator of turbulence suppression as a function of the wall distance. Even at the largest applied stratification, no relaminarization was observed in Refs. [118] and [119]. Similar results were also obtained by other researchers carrying experiments in wind tunnels or open channels (see for instance Refs. [120] and [121]). More recently, a series of wind tunnel experiments performed by Ohya et al. [122–124] extended the previous investigations considering both smooth and rough boundaries and covering a wider range of stratification levels. In the 1997 paper, Ohya et al. [122] focused on turbulent boundary layers developed over a smooth surface and reported a significant decrease of velocity/temperature fluctuations and turbulent fluxes for increasing stratification. Under very strong stratification, velocity and temperature fluctuations vanished even close to the boundary and flow relaminarization occurred. In the 2001 paper, Ohya [124] extended the previous results considering the stratified boundary layer over a rough surface (chain roughness). While under weak stratification turbulence is enhanced by surface roughness, it is completely suppressed under strong stratification.

4.2 Field Measurements. Field measurements of wall-bounded stratified turbulence (chiefly in the ocean and in the atmosphere) are particularly difficult due to the complex surface morphology and to the inherent difficulties in measuring turbulence scales at large Reynolds number [108,125]. Two important field programs, called SABLES-98 and CASES-99, were run few years ago to characterize the atmospheric boundary layer. The SABLES-98 experiment (Stable Atmospheric Boundary Layer Experiment in Spain-1998 [99]) took place in September 1998 in a broad flat region located in the north of Spain. During the 14 nights (12 h long) of experiments, different stratified conditions were sampled by a 100-m tower, ranging from near neutral to strongly stable. The second experiment, CASES-99 (Cooperative

Atmosphere-Surface Exchange Study 1999 [100]), was held in October 1999 in south-eastern Kansas, in the Great Plains of the U.S. The nights were about 13 h long, and the winds were generally stronger than those of the SABLES-98 campaign. The tower was 60-m high and very densely instrumented. Thanks to the previous campaigns of field measurements, a detailed characterization of heat/momentum fluxes, intermittency, and turbulent mixing was possible. Hints on the applicability of the Monin–Obukhov similarity theory under weakly and strongly stratified conditions as well as the role of surface heterogeneity were also given.

In the ocean, field measurements are inherently more difficult than in the atmosphere and are usually limited to the vertical distribution of mean temperature using shipborne conductivity, temperature, depth [31,126,127]. Measurements of the mean temperature profile are important since they can be effectively used as an indirect measure of the turbulent dissipation rate [28,29,128], a key parameter to estimate the global energy budget in the ocean as well as to quantify mixing and vertical diffusivity of species. An example of the temperature distribution obtained during an oceanic experimental campaign is provided in Fig. 5 (taken from Cimattoribus et al. [126]). The time behavior of temperature, measured by thermistors distributed from the surface down to the ocean bottom (the first thermistor is approximately 5 m above the bottom), is shown during a downslope (decreasing temperature) and an upslope (increasing temperature) tidal phase. When a more precise estimate of the dissipation rate is required, velocity gradients must be measured at the millimeter scale through temperature/velocity profiling devices with sensitive high-speed thermistors and thin films (see the reviews of Wunsch and Ferrari [7] and Ivey et al. [125] for further details). Note that a direct estimate of mixing can be accessed via tracer-release experiments (we refer the reader to [125,129,130] and references therein), realized by injecting an inert dye in a controlled fashion into the ocean at depth, and tracking its subsequent evolution.

Although field measurements at the dissipation scale remain a challenge for most of the commonly used probing instruments, more recent techniques like airborne Doppler lidar, remote turbulence/temperature profilers, or shipborne microstructure facilities promise to open new frontiers in the field observations of wall-bounded stratified turbulence [7,108,131].

5 Flow Structure of Wall-Bounded Stratified Turbulence

In this section, we review some of the main scientific results obtained by studies on wall-bounded stratified turbulence. Many

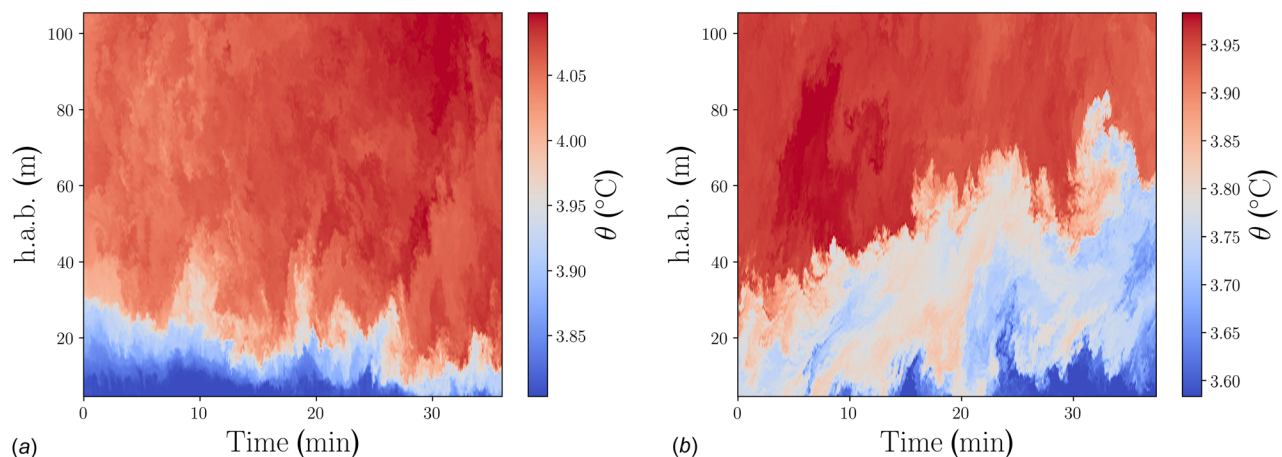


Fig. 5 Time measurements of the temperature as a function of the distance from the bottom boundary (h.a.b.) during an experimental campaign focused on the bottom oceanic boundary layer. (Reproduced with permission from Cimattoribus and van Haren [125]. Copyright 2015 by Cambridge University.)

of the results we will discuss have been obtained by numerical simulations, which have the advantage of providing not only a measure of global mean quantities, but also an accurate characterization of the local flow structure. Here, we clearly distinguish between weakly/moderately stratified flows and strongly stratified flows, since the relevant flow phenomenology is substantially different.

5.1 Weakly/Moderately Stratified Turbulence. The first numerical study analyzing wall-bounded stratified turbulence in a systematic fashion was done by Garg et al. [44], who performed wall-resolved LES of incompressible stratified turbulence in both close and open channel flow configurations at a constant Re_τ and Pr number but at different Ri_τ (i.e., different stratification levels). The occurrence of three different regimes was observed, depending on the value of Ri_τ : a buoyancy-affected regime ($Ri_\tau < 30$), with turbulence partially suppressed; a buoyancy-controlled regime ($30 < Ri_\tau < 45$), with a temporary flow relaminarization in one half of the channel followed by a sharp transition restoring a symmetric turbulent flow; a buoyancy-dominated regime ($Ri_\tau > 45$), with a rapid relaminarization of the whole flow. Similar results, showing one-sided turbulence with local flow laminarization, were observed by Iida et al. [75] in their OB-approximated-DNSs of stratified channel turbulence at $Re_\tau = 150$ and $Ri_\tau = 40$. However, findings of Refs. [44] and [75] were in apparent contradiction with the linear stability analysis [68], with this latter predicting much larger values of the imposed stratification (compared to those considered by Garg et al. [44] and Iida et al. [75]) for the flow to become laminar. To identify the reason of this discrepancy, Armenio and Sarkar [18] performed a wall-resolved LES of stratified channel turbulence at $Re_\tau = 180$ and different values of the imposed stratification in the range $0 < Ri_\tau < 480$. They noticed that the flow laminarization for subcritical values of Ri_τ (see Sec. 3.1 for a proper definition of critical and subcritical) observed in Refs [44] and [75] was just a transient effect disappearing after a sufficient time. A clearcut explanation of these important differences was given recently by García-Villalba and del Álamo [45]. Performing DNS of stratified channel turbulence up to $Re_\tau = 550$ and $Ri_\tau = 960$, and employing larger computational domains, García-Villalba and del Álamo were able to show that local flow laminarization for subcritical values of Ri_τ occurs only when the computational domain is not large enough to contain the minimal flow unit required to sustain turbulence. In this case, laminar patches appear, increase in size, and become large enough to forbid a back transition to turbulence. Therefore, when the flow domain is too small, a complete relaminarization occurs at one (or both) side of the channel even at subcritical values of Ri_τ . In summary, García-Villalba and del Álamo have shown that contradictions with linear stability analysis is only a numerical outcome due to the subminimal size of the computational domain.

It is now widely accepted [132,133] that unstratified near-wall turbulence is characterized by a broad range of spatial structures. At one extreme, there are near-wall streaks having a streamwise length of approximately $\lambda_x \simeq 10^3$ wall units and spanwise width of $\lambda_y \simeq 10^2$ wall units. At the opposite extreme, there are very large and tall structures called global modes and characterized by $\lambda_x \simeq 10h$ and spanwise width of $\lambda_y \simeq 2h$. Contour plots of the streamwise velocity fluctuations, taken from García-Villalba and del Álamo [45], are shown in Fig. 6 to give a flavor of near wall turbulence structures. Figure 6(a) refers to unstratified turbulence, while Fig. 6(b) refers to stratified turbulence at $Re_\tau = 550$ and $Ri_\tau = 480$. Dark streaks indicate low-speed regions while light streaks indicate high speed regions. The cutting plane is located at $z^+ = 15$. The vis-a-vis comparison between unstratified and stratified case demonstrates that near wall streaks are only slightly influenced by the imposed stratification (i.e., streaks slightly narrow). Differently from the near wall streaks, global modes generated by very large and tall structures extending well into the outer

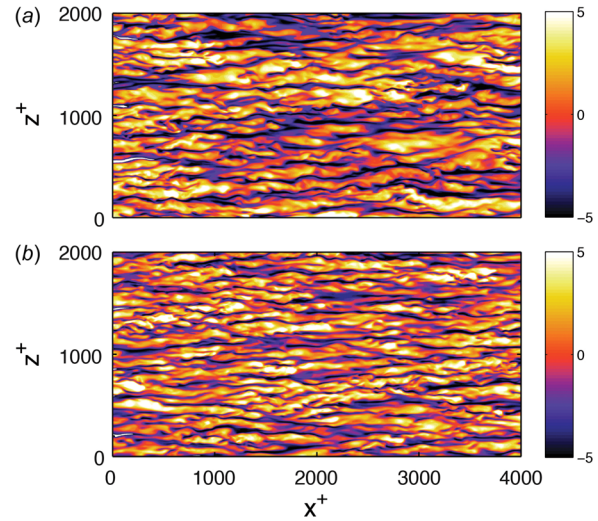


Fig. 6 Contour map of the streamwise velocity fluctuations on a x - y plane in the near wall region ($z^+ \simeq 15$) for $Re_\tau = 550$. Panel (a): unstratified flow; Panel (b): stratified case at $Ri_\tau = 480$. (Reproduced with permission from García-Villalba and Álamo [45]. Copyright 2011 by AIP Publishing.)

region of the boundary layer are influenced by stratification [45]. Moving toward the core of the channel, the dynamics of the flow becomes completely different, as stratification starts influencing the larger flow scales first, the smaller later. The dominant structures in this region are strong nonturbulent motions called IGWs. Contour maps of density (Fig. 7(a)) and wall-normal velocity fluctuations (Fig. 7(b)) at the channel center taken from García-Villalba and del Álamo [45] are presented, precisely to visualize IGW. The black thick line refers to the position of a crest of the density isosurface, $\partial\rho/\partial x = 0$. Density and vertical velocity fluctuations are characterized by very similar, although shifted, patterns [30,45,75]. As explicitly quantified by Iida et al. [75], and reported in Fig. 8, the phase shift approaches $\pi/2$ at the channel center (i.e., at $y^+ = 150$). The presence of this phase shift explains why, although temperature and wall-normal velocity fluctuations at the channel core are large, turbulent fluxes remain very small [18,45,75].

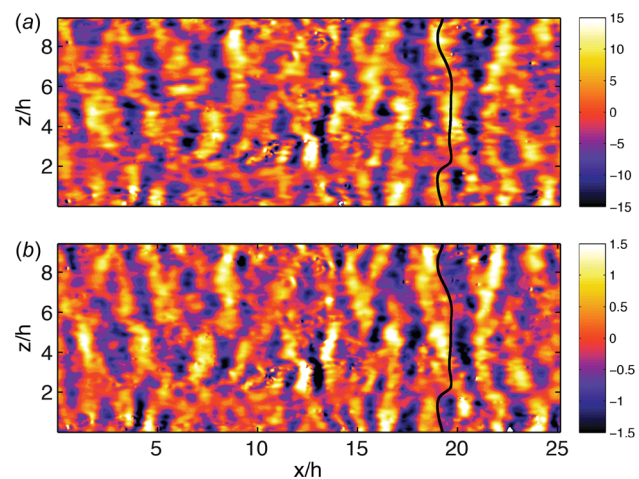


Fig. 7 Contour map of density (panel a) and wall normal velocity fluctuations on a horizontal plane at the center of the channel for $Re_\tau = 550$ and $Ri_\tau = 480$. The black solid line indicates the trace $\partial\rho/\partial x = 0$ obtained after smoothing the temperature field by 2D cutoff filter. (Reproduced with permission from García-Villalba and Álamo [45]. Copyright 2011 by AIP Publishing.)

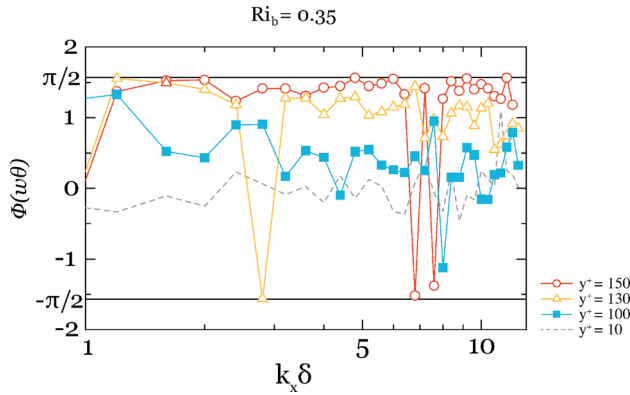


Fig. 8 Behavior of the phase angle $\phi(w\theta)$ between the vertical velocity w and the temperature fluctuations θ as a function of the normalized wavenumber in the streamwise direction $k_x \delta$. Measurements are taken at different locations from the wall (y^+) for moderately stratified conditions. (Reproduced with permission from Iida et al. [75]. Copyright 2002 by Elsevier.)

The origin of internal waves is the restoring effect due to buoyancy. A fluid particle with density $\bar{\rho}(z_0)$ that is displaced vertically of a distance ζ by velocity fluctuations, finds itself surrounded by a fluid having density $\bar{\rho}(z_0 + \zeta) = \bar{\rho}(z_0) + \zeta d\bar{\rho}(z_0)/dz$. A force balance on the fluid particle gives

$$\begin{cases} \frac{d^2 \zeta}{dt^2} + N^2 \zeta = 0 \\ N = \sqrt{-\frac{g}{\bar{\rho}(z_0)} \frac{d\bar{\rho}(z_0)}{dz}} \end{cases} \quad (17)$$

This equation describes the oscillating motion of a fluid particle around its equilibrium position at frequency N , which is usually called Brunt-Väisälä (or simply buoyancy) frequency. For an in-depth analysis of IGWs and their importance, we refer the reader to previous references [7,20,48,134–136]. Internal waves can be considered a sort of thick interface characterized by the presence of strong temperature/density gradients (usually called thermocline or pycnocline, see Refs. [23] and [36]) and largely influencing the mixing properties of the flow. To measure the amount of mixing, the concept of mixing efficiency, i.e., the efficiency with which the density field in stably stratified fluid is mixed by turbulent processes, is commonly invoked [15,137]. Mixing efficiency is often estimated via the flux Richardson number $Ri_f = B_k/P_k$, which is the ratio of buoyancy destruction flux (B_k) to shear production (P_k) in the turbulent kinetic energy equation. Although the experimental and numerical results on mixing are characterized by a significant spread, it is now widely accepted that Ri_f is characterized by a nonmonotonic behavior when expressed as a function of the bulk Richardson number, Ri_b : for increasing Ri_b (increasing stratification), Ri_f initially increases, reaches a maximum value $Ri_f \simeq 0.2$, and later decreases (see for instance [15,18,69,108,137]). Note that R_f can be negative in nonstationary flows [104] or highly stratified channel flows characterized by higher countergradient fluxes [18], while it can exceed unity for high gradient Richardson numbers [45]. More appropriate definition of the mixing efficiency based on irreversible mixing and viscous dissipation of the turbulent kinetic energy are available (we refer the reader to the review paper by Peltier and Caulfield [137] on this topic).

5.2 Strongly Stratified Turbulence. Differently from the weakly/moderately stratified regime, for which reliable theories and parametrizations exist, the case of strongly stratified wall-bounded flows remains more elusive. As documented in an

important sequence of DNS studies and experiments [14,45,69–71,77,122,124], in strongly stratified conditions buoyancy effects become so strong to influence not only the flow region far from the boundary, but also that close to the boundary. Under strongly stratified conditions, near wall turbulence collapses leading to the corresponding appearance of long laminar patches. Figure 9, taken from Brethouwer et al. [70], shows contour maps of the streamwise velocity monitored in a horizontal plane parallel to the boundary and located at a distance of 10 wall units. The results refer to different stratification levels, namely $Re_\tau = 80$ and $Ri_\tau = 0$ for panel (a), $Re_\tau = 113$ and $Ri_\tau = 38$ for panel (b), $Re_\tau = 192$ and $Ri_\tau = 273$ for panel (c), and finally $Re_\tau = 334$ and $Ri_\tau = 985$ for panel (d). While for unstratified conditions, the typical near wall structure consisting of low and high speed streaks is recovered, for strongly stratified conditions laminar regions emerge within a network of turbulent patches. The distribution of these turbulence patches may change from case to case, ranging from irregular to randomly distributed patterns, up to inclined stripes [45,69–71,77]. The distribution of laminar and turbulence patches influences in a complex fashion also the structure in the bulk of the flow. For smaller Re_τ , laminar regions span vertically the entire domain depth, whereas for larger Re_τ laminar regions seem more confined to the wall, with the interior part of the domain remaining turbulent [69,70].

The problem of turbulence collapse under strongly stratified conditions has been originally analyzed using field measurements at high Re . The stability parameter introduced to characterize the tendency of the flow to suppress turbulence motions and to enter the laminarization process was based on the Monin–Obukhov length scale L_{MO} . Based on the data obtained by the microfronts experimental campaign [138], Mahrt [139] proposed $\delta/L_{MO} \simeq 1$, with δ the thickness of the turbulent boundary layer, as a threshold value between the weakly and strongly stratified regimes. A slightly different threshold value, $\delta/L_{MO} \simeq 0.5$, was instead proposed by Hogstrom [140] reviewing data from different experimental campaigns. Performing a series of wind tunnel experiments at fairly high Reynolds numbers ($Re_\tau = 1000/4000$), Ohya and coworkers [122,124] found larger values of the critical parameter h/L_{MO} ($h/L_{MO} \simeq 5$ for smooth surface, $h/L_{MO} \simeq 2$ for rough surfaces) for the onset of turbulence collapse. In this case, the tunnel height h was taken as reference. According to the measurements done during the field program CASES-99 [100], flow intermittency starts at $\delta/L_{MO} \simeq 3$, while total turbulence suppression at the ground occurs for $\delta/L_{MO} \simeq 10^3$ [141]. Few years later, Nieuwstadt [14] performed DNS of strongly stratified flow inside an open channel at $Re_\tau = 360$ and presented evidence for relaminarization for $h/L_{MO} \simeq 1/2$ (with h the half channel height).

The lack of precise values of h/L_{MO} (or δ/L_{MO}) to determine the onset of turbulence collapse indicated that h/L_{MO} was not the right parameter for the scope. The issue was solved only recently by Flores and Riley [77], who argued that the laminarization process is intimately linked to the dynamics of the near-wall structures and should therefore scale with inner variables (rather than with outer variables). Instead of using the h/L_{MO} criterion, Flores and Riley proposed the adoption of the L_{MO}^+ criterion, where $L_{MO}^+ = L_{MO} u_\tau / \nu$ is the Monin–Obukhov length scale normalized in wall units. With the new rescaling, a threshold value $L_{MO}^+ \simeq 100$ was found for turbulence to collapse [77]. The criterion for turbulence collapse proposed by Flores and Riley [77] was later confirmed by Deusebio et al. [69], who however slightly modified the estimate for the critical value to $L_{MO}^+ \simeq 200$. Interestingly, they also noticed that the appearance of local flow laminarization does not have a significant effect on the value of the overall mixing efficiency, possibly due to the simultaneous reduction of both buoyancy flux and shear production (their ratio remaining almost constant). It is worth noting that the choice of the domain size in numerical simulations of strongly stratified turbulence is even more important than for weakly/moderately stratified flows (see in particular the discussion in Refs. [45] and [70]).

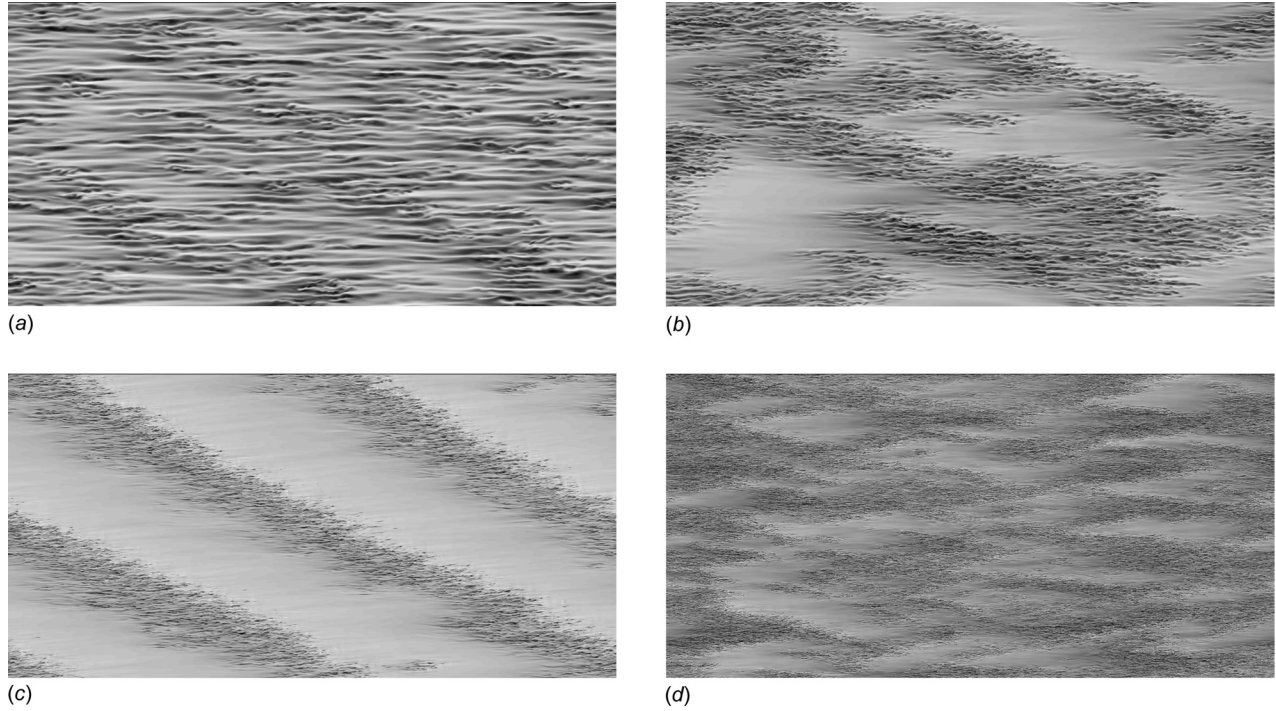


Fig. 9 Contour map of the streamwise velocity u_x on a horizontal parallel plane located at 10 wall units from the wall. Panels are as follows: panel (a) $Re_\tau = 80$ and $Ri_\tau = 0$; panel (b) $Re_\tau = 113$ and $Ri_\tau = 38$; panel (c) $Re_\tau = 192$ and $Ri_\tau = 273$; panel (d) $Re_\tau = 334$ and $Ri_\tau = 985$. (Reproduced with permission from Brethouwer et al. [70]. Copyright 2012 by Cambridge University.)

6 Influence of Stratification on Macroscopic Heat and Momentum Transfer Rates

In this section, we review one of the most fundamental problem that attracted attention of researchers due to its practical and technological importance: how heat and momentum transfer rates are modified by stratification in a turbulent channel. Heat and momentum transfer rates are commonly quantified by the Nusselt number, Nu , which measures the convective to conductive heat transfer ratio, and the friction factor C_f , which measures the shear stress to the kinetic energy ratio. Here, the following definitions are used [45,116]

$$\begin{cases} Nu = \frac{2q_w h}{\lambda \Delta T} \\ C_f = \frac{2\tau_w}{\rho u_b^2} \end{cases} \quad (18)$$

where q_w is the wall heat flux. The results obtained from both numerical simulations [6,35,44,45,116] (filled symbols) and experimental measurements [119,142] (open symbols) for Nu and C_f are shown in Fig. 10 as a function of the shear Richardson number Ri_τ . As was originally reported in experiments [118,119], and later confirmed by simulations [18,44,45,75,116], stratification reduces wall-normal heat and momentum transfer rates compared to the neutrally buoyant case ($Ri_\tau = 0$), since the potential energy toll required to stir the mean shear increases for increasing stratification [45]. Based on their DNS database, García-Villalba and del Álamo [45] noticed that the bulk Richardson number scales as $Ri_b \propto Ri_\tau^2/3$, and considering that $C_f/4 = Ri_b/Ri_\tau$, they finally obtain $C_f \propto Ri_\tau^{-1/3}$. This scaling law is also shown in Fig. 10(a). Although at present a proper theoretical justification for this law is still missing, it seems to predict fairly well the behavior of C_f even for larger Reynolds and Richardson number.

Differently from C_f , for which all gathered data seem to collapse onto a unique functional relationship $C_f = f(Ri_\tau)$, for the Nusselt number this collapse is not recovered. In particular, the

available literature results indicate that the Nusselt number increases for increasing Re_τ , as indicated by the arrow in Fig. 10(b). We remark that a universal parametrization of Nu for stratified flows is still to be obtained, with current estimates being based on the value of the transfer coefficients obtained from the unstratified case [116].

7 Recent Results on Non-Oberbeck–Boussinesq Effects

When stratification is characterized by non-negligible variations of the fluid properties, predictions obtained with the OB approximation may be largely inaccurate, with correspondingly different flow phenomenology. Indeed in this case, if the fluid is a gas, compressibility effects will become more important than other effects, whereas if the fluid is a liquid, effects due to temperature-dependent variations of viscosity, thermal expansion coefficient, and specific heat will be predominant. It is clear at this stage that the balance equations describing the flow are different, as discussed in Sec. 2. In this section, we review relevant studies that analyzed stratified wall-bounded turbulence with several approaches that are not based on the OB approximation. Because these approaches are not unified and are based on different hypotheses, we follow the general custom and we define all these approaches NOB.

Garg et al. [44] were among the first performing LES of an open channel and assuming temperature dependent viscosity and diffusivity. Due to the low influence of temperature on the thermophysical properties of air, flow changes were however rather limited. Later, Lessani and Zainali [143] used a Low-Mach number approach to perform LES of an air flow ($Pr = 0.71$) inside a closed channel at moderately Reynolds number $Re_\tau = 180$ and considering a wide range of temperature ratio between the hot and cold wall, from 1.01 to 6. In this case, the nonuniform distribution of the fluid properties (in particular at the largest temperature gradients), induced a strong flow asymmetry characterized by local flow laminarization near the hot wall. This of course had

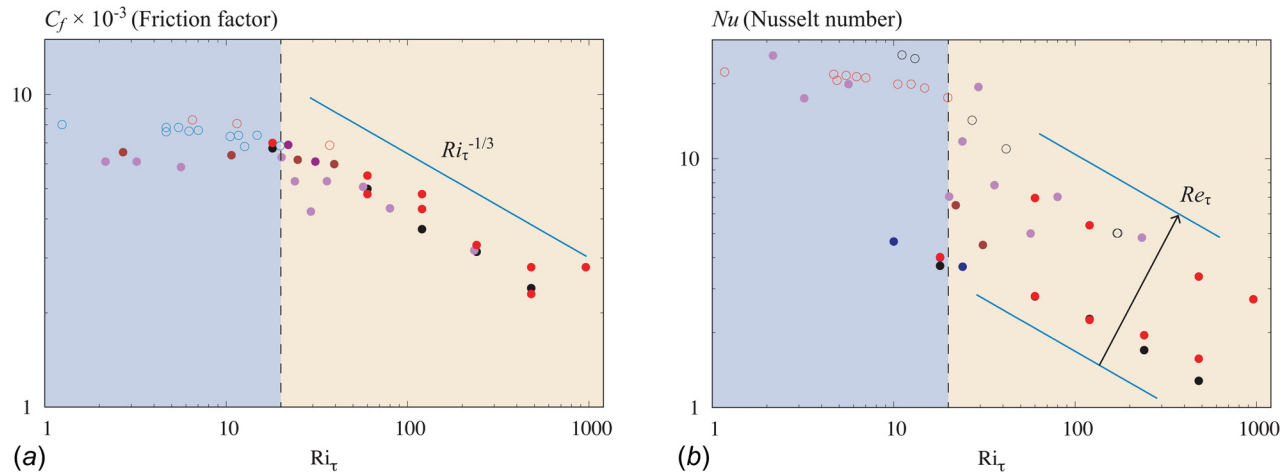


Fig. 10 Panel (a) behavior of the friction factor C_f as a function of the shear Richardson number Ri_τ . Panel (b) behavior of the Nusselt number, Nu , as a function of the shear Richardson number Ri_τ . Data are gathered both from numerical [6,35,44,45,116] (filled symbols) and experimental studies [119,142] (open symbols).

implications on the heat/momentum transfer rates and on the mixing efficiency.

A problem that is attracting increasing interest is the heat transfer process in a turbulent flow of supercritical carbon dioxide (sCO_2). Bae et al., [40,144] simulated the heat transfer for sCO_2 at 8 MPa in a pipe and annular geometry at bulk Reynolds number $Re = 5400/8900$, with gravity parallel to the wall. These authors report a significant influence on velocity and shear stress profiles as well as decreased vortical motions near the heated surface. Since streamwise vortices play a key role in the self-regenerating process of near-wall turbulence [145,146], their modulation remarkably influences the entire flow phenomenology. More recently, Nemati et al. [42] and Peeters et al. [147] focused on a similar flow configuration, though at bulk Reynolds number, $Re = 8000$. Statistics of turbulent shear stress, turbulent heat flux, and turbulent kinetic energy were found to depend strongly on the nonuniform distribution of the material fluid properties. Figure 11,

taken from Ref. [147], shows indeed the instantaneous distribution of density, viscosity, and Prandtl number (all depending on temperature) in the annulus for the forced convection case (i.e., buoyancy is neglected, case II of Ref [147] shown in Fig. 11(a)) and for the mixed convection case (i.e., buoyancy is accounted for, case III in Ref. [147] shown in Fig. 11(b)). The results indicated that production of turbulent kinetic energy was decreased near the hot inner wall and increased near the cold outer wall.

When NOB effects are analyzed for liquids far from their critical point, density in the continuity equation can be considered uniform and constant, while the temperature variation of the other fluid properties must be taken into account. This approach was used by Zonta et al. [36,116] to perform DNS of a turbulent channel flow of water at moderate Reynolds numbers (up to $Re_\tau = 180$). In this study, the dependencies of the fluid properties were implemented one at a time as a function of the local fluid temperature. Such procedure allows explicating the importance of

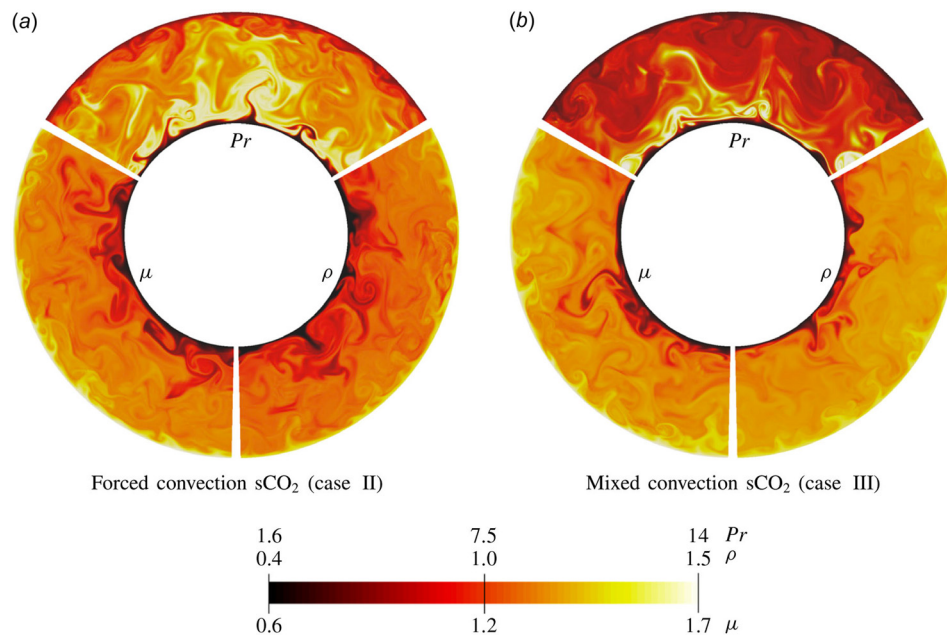


Fig. 11 Distribution of density ρ , viscosity μ and Prandtl number Pr of supercritical CO_2 in a cross section of an annular pipe heated from the inner wall and cooled from the outer wall. Panel (a) refers to the forced convection case (no buoyancy); panel (b) refers to the mixed convection case (buoyancy is accounted). (Reproduced with permission from Peeters et al. [70]. Copyright 2016 by Cambridge University.)

the variation of each single property, one independently to each other, on the overall NOB effects. It was explicitly shown that high-viscosity regions hinder turbulence activity (possibly leading to a local flow relaminarization), while low-viscosity regions promote turbulence activity. A temperature-dependent thermal expansion coefficient was shown to produce an opposite effect (reducing turbulence when larger, while promoting it when smaller). From the previous overview, it is apparent that NOB effects depend strongly on the employed working fluid, since gradients of a specific fluid properties can be dominant in one case while negligible in others. In particular, for small Re_τ , the effects of large property gradients can overwhelm the effects of gravity. In this case, the local Reynolds number (or its wall-normal gradient) can be used to describe carefully the near-wall turbulence dynamics [148]. If the local Reynolds number decreases away from the wall (air flow over cold surface), then coherent structures are sustained; by contrast, when the Reynolds number increases away from the wall (water over cold surface), a higher inter-component energy transfer is likely to occur. All the investigations performed under the OB approximation have contributed to provide a general framework to deepen our understanding of wall-bounded stably stratified Turbulence. And this framework is an important point to start examining effects that are not here comprised. Elaborating a bit further, whereas the values of the dimensionless numbers are fully representative of the physical instance examined under the OB approximation, this is not the case when the OB approximation is trespassed: in this case, it is in fact necessary to fully specify not only the values of the reference physical properties involved (ρ_0 , μ_0 , $c_{p,0}$, etc.) but also their dependency on the main state variables (i.e., p and T).

8 Conclusions

The status of current understanding of wall-bounded turbulent stratified flows has been reviewed in this work starting from the first important contributions appeared in the fifties [21,25]. In this type of flows, there is a competition between inertial and buoyancy forces, and it is customary to use this inertial and buoyancy forces balance to classify such flows: when inertial forces dominate over buoyancy forces—the weakly/moderately stratified case—turbulence is actively sustained near the boundary, whereas we observe the appearance of large nonturbulent wavy structures, called IGWs, far from the boundary. This regime is by and large the most investigated regime, bearing important consequences in a number of environmental and industrial phenomena. When buoyancy forces dominate—the strongly stratified case—their influence reaches down to the boundary, and in extreme conditions can lead to complete suppression of the turbulence regeneration cycle [145,146]. However, when buoyancy forces are not sufficiently strong to fully suppress the turbulence regeneration cycle, these flows can exhibit intermittent turbulent patches and patterns which have been given attention in recent papers.

The complex mutual interactions between inertial, buoyancy and viscous forces in wall bounded stratified turbulence gives rise to a number of length scales relevant to describe the observed phenomena. In addition to the usual Kolmogorov scale used to measure the minimum size of eddies that can be sustained by turbulence without being dissipated by viscosity, wall bounded stratified turbulence can be characterized by the Ozmidov scale, which estimates the size of the smallest eddies influenced by buoyancy. Naturally, in regions where the Ozmidov scale is larger than the Kolmogorov scale, the flow is turbulence-dominated, and this usually happens near the boundary. In regions where the Ozmidov scale is smaller than the Kolmogorov scale, the flow is buoyancy-dominated, and this usually happens far from the boundary.

In the framework of this work, we also considered important to review early predictions based on the linear stability analysis [67,68], which have been used to estimate the maximum level of stratification for which turbulence is still active and not completely suppressed. These analyses have been also instrumental to

stimulate a number of subsequent simulations performed to investigate numerically these limits.

A large proportion of the papers reviewed is based on the OB approximation: in this way, the governing balance equations are greatly simplified, and relevant numerical simulations have been able to reveal important features of stratified turbulent flows. However, the range of validity of this approximation cannot be stretched without incurring into possible wrong predictions, and more complex non-Oberbeck–Boussinesq approaches must be employed. In these approaches, the thermodynamic variables vary as a function of temperature and/or pressure, hence requiring ad hoc numerical treatments. The low-Mach number and the incompressible non-Oberbeck–Boussinesq approximations are more and more employed to these purposes, and have recently been used to discover important features of wall-bounded turbulent stratified flows. The more important points are summarized in Fig. 12.

SUMMARY POINTS

- 1
 Wall-bounded turbulent stratified flows are classified into weakly/moderately stratified and strongly stratified. In weakly/moderately stratified flows, turbulence is active near the boundary, and exhibit large non-turbulent wavy structures called Internal Gravity Waves (IGW) far from the boundary. In strongly stratified flows, buoyancy effects influence also the region close to the boundary, producing complex flow patterns characterized by the presence of laminar patches surrounded by regions in which turbulence is reactivated.
- 2
 Estimates, based on linear stability analysis and simulations, are available to predict whether the stratified flow is able to sustain turbulence or not (i.e. becoming fully laminar).
- 3
 Analysis of stratified turbulence is customarily done introducing the Oberbeck–Boussinesq (OB) approximation, which greatly simplify the governing equations. When the OB approximation is not physically justified, more complex Non-Oberbeck–Boussinesq (NOB) approaches (Low-Mach number approximation, Incompressible Non-Oberbeck–Boussinesq) must be used.
- 4
 Stratification modifies heat and momentum transfer rates, ultimately influencing friction factor and Nusselt number. Compared to the neutrally-buoyant case (where temperature is considered a passive scalar) friction factor and Nusselt number decrease.
- 5
 The structure of a wall-bounded stratified flow can be inferred from the relative importance of the Ozmidov and Kolmogorov scales. In regions where the Ozmidov scale is larger than the Kolmogorov scale, the flow is turbulence-dominated, and this usually happens in the near wall region. In regions where the Ozmidov scale is smaller than the Kolmogorov scale, the flows is buoyancy-dominated, and this usually happens in the core region.

Fig. 12 Summary points at a glance

FUTURE CHALLENGES AND PERSPECTIVES

1 Analyses carried employing Direct Numerical Simulations (DNS) have elucidated important physics in the context of stably stratified wall bounded turbulence, but the Reynolds number in available studies is yet too small compared to that characterizing full scale environmental and industrial phenomena. And there is indeed no absolute certainty that low Reynolds number simulation results can be upscaled to the relevant scales of the real phenomena, especially in oceanic and atmospheric instances. A bright future for the largest exa-scale DNS to be run on the present day available big supercomputers is foreseen.

2 Although the Oberbeck-Boussinesq (OB) approximation has been of enormous importance to resolve the first doubts in stratified wall turbulence, computational tools are now available to explore such flows under the Non-Oberbeck-Boussinesq (NOB) approach. This approach is inevitable when large temperature gradients exist and/or when the focus is on phenomena occurring at large vertical scales.

3 Current modeling approaches, based on LES and RANS, to study strongly stratified wall bounded flows are not fully reliable. A sharp improvement of these modeling techniques is therefore required.

4 Further attention is required by physical situations in which the fluid density depends on two scalar fields (double diffusive convection). These complex situations are ordinary occurrences in oceans, where temperature gradient is the stabilizing factor and salinity gradient produces instabilities. We consider DNS developments for double diffusive convection of paramount importance for in-depth physical environmentally-relevant analyses.

5 A very active field of research, which is crucially important for geophysical and environmental applications, is the stratified rotating Ekman layer. In such flow instance, buoyancy effects interact with rotational effects to produce complex and hard to predict physics. The investigated range of the governing parameters (Reynolds number, Richardson number and Rossby number – for the rotation) is clearly too limited and must be extended.

Fig. 13 Future challenges and perspectives *at a glance*

9 Future Issues

Although experimental, computational, and theoretical methodologies have provided us with plentiful data and insights in the complex intertwined phenomena characteristic of buoyancy-influenced turbulent bounded flows, the field remains rich in future challenges.

In the framework of the numerical approaches, DNS has certainly provided to be the most generous source of information.

But the Reynolds number in the available studies is yet too small to satisfy the urge for answers posed by full-scale environmental and industrial phenomena. There is in fact no absolute certainty that low Reynolds number simulation results can be upscaled to the relevant scales of the real phenomena, especially in oceanic and atmospheric instances. We envision a bright future for the largest exa-scale DNS to be run on the present day available big supercomputing facilities. These will allow for systematic investigations in the parameter space for a tenfold increase of the relevant dimensionless numbers. The large-scale databases produced within the new computational environment will definitely help LES to build long desired and reliable subgrid scale models. We believe that RANS also benefit from these new databases to develop buoyancy-influenced turbulence closure laws.

Although the Oberbeck–Boussinesq approximation has always been a powerful tool to resolve the first doubts in stratified wall turbulence, computational tools are available to explore such flows under the non-Oberbeck–Boussinesq approach. This approach is inevitable when large temperature gradients exist and/or when the focus is on phenomena occurring at large vertical scales.

Further attention is required by physical situations in which the fluid density depends on two scalar fields (double diffusive convection). These complex situations are ordinary occurrences in oceans, where temperature gradient is the stabilizing factor, and salinity gradient produces instabilities. Different rates of temperature and salt diffusivity makes the fluid dynamics particularly rich and hard to capture [149,150]. Although we did not cover these problems in the present review, we consider DNS developments for double diffusive convection of paramount importance for in-depth physical environmentally relevant analyses.

Finally, and yet not covered in this present review, is the stratified rotating Ekman layer, which is crucially important for geophysical and environmental applications. In such flow instance, buoyancy effects interact with rotational effects to produce complex and hard to predict physics [151–153]. The investigated range of the governing parameters (Reynolds number, Richardson number and Rossby number—for the rotation) is clearly too limited and must be extended.

This view on challenges and perspectives in the field of wall bounded turbulent stratified flows is summarized in a graphical way in Fig. 13 so to be captured *at a glance* by the reader.

Acknowledgment

The authors thank Professors Manuel García-Villalba and Rene Pecnik for their helpful comments on the first draft of this paper. The authors also thank colleagues who allowed the use of their images in this review and all those who provided advice and suggestions on the manuscript. CINECA supercomputing center (Bologna, Italy), Vienna Scientific Cluster (Vienna, Austria) and Argonne National Lab (Argonne, USA) are also gratefully acknowledged for generous allowance of computer resources.

References

- [1] Dostal, V., Hejzlar, P., and Driscoll, M., 2006, "The Supercritical Carbon Dioxide Power Cycle: Comparison to Other Advanced Power Cycles," *Nucl. Technol.*, **154**(3), pp. 283–301.
- [2] Pitla, S. S., Robinson, D. M., Groll, E. A., and Ramadhyani, S., 2006, "Heat Transfer From Supercritical Carbon Dioxide in Tube Flow: A Critical Review," *HvacR Res.*, **4**(3), pp. 281–301.
- [3] Zonta, F., Marchioli, C., and Soldati, A., 2008, "Direct Numerical Simulation of Turbulent Heat Transfer Modulation in Micro-Dispersed Channel Flow," *Acta Mech.*, **195**(1–4), pp. 305–326.
- [4] Galizzi, C., and Escudé, D., 2010, "Experimental Analysis of an Oblique Turbulent Flame Front Propagating in a Stratified Flow," *Combust. Flame*, **157**(12), pp. 2277–2285.
- [5] Mahrt, L., 2014, "Stably Stratified Atmospheric Boundary Layers," *Annu. Rev. Fluid Mech.*, **46**(1), pp. 23–45.
- [6] Williamson, N., Armfield, S. W., Kirkpatrick, M. P., and Norris, S. E., 2015, "Transition to Stably Stratified States in Open Channel Flow With Radiative Surface Heating," *J. Fluid Mech.*, **766**, pp. 528–555.

- [7] Wunsch, C., and Ferrari, R., 2004, "Vertical Mixing, Energy, and the General Circulation of the Oceans," *Annu. Rev. Fluid Mech.*, **36**(1), pp. 281–314.
- [8] Lilly, D. K., 1983, "Stratified Turbulence and the Mesoscale Variability of the Atmosphere," *J. Atmos. Sci.*, **40**(3), pp. 749–761.
- [9] Riley, J. J., and Lelong, M.-P., 2000, "Fluid Motion in the Presence of Strong Stable Stratification," *Annu. Rev. Fluid Mech.*, **32**(1), pp. 613–657.
- [10] Lindborg, E., 2006, "The Energy Cascade in a Strongly Stratified Fluid," *J. Fluid Mech.*, **550**(1), pp. 207–242.
- [11] Smyth, W. D., and Moun, J. N., 2000, "Length Scales of Turbulence in Stably Stratified Mixing Layers," *Phys. Fluids*, **12**(6), pp. 1327–1342.
- [12] Smyth, W. D., and Moun, J. N., 2000, "Anisotropy of Turbulence in Stably Stratified Mixing Layers," *Phys. Fluids*, **12**(6), pp. 1343–1362.
- [13] Cortesi, A., Yadigaroglu, G., and Banerjee, S., 1998, "Numerical Investigation of the Formation of Three-Dimensional Structures in Stably-Stratified Mixing Layers," *Phys. Fluids*, **10**(6), pp. 1449–1473.
- [14] Nieuwstadt, F. T. M., 2005, "Direct Numerical Simulation of Stable Channel Flow at Large Stability," *Boundary Layer Meteorol.*, **116**(2), pp. 277–299.
- [15] Fernando, H. J. S., 1991, "Turbulent Mixing in Stratified Fluids," *Annu. Rev. Fluid Mech.*, **23**(1), pp. 455–493.
- [16] Rohr, J. J., Itsweire, E. C., Helland, K. N., and van Atta, C. W., 1988, "Growth and Decay of Turbulence in a Stratified Shear Flows," *J. Fluid Mech.*, **195**(1), pp. 77–111.
- [17] Holt, S. E., Koseff, J. R., and Ferziger, J. H., 1992, "A Numerical Study of the Evolution and Structure of Homogeneous Stably Stratified Sheared Turbulence," *J. Fluid Mech.*, **237**(1), pp. 499–539.
- [18] Armenio, V., and Sarkar, S., 2002, "An Investigation of Stably Stratified Turbulent Channel Flow Using Large-Eddy Simulation," *J. Fluid Mech.*, **459**, pp. 1–42.
- [19] Mahrt, L., 1999, "Stratified Atmospheric Boundary Layers," *Boundary Layer Meteorol.*, **90**(3), pp. 375–396.
- [20] Staquet, C., and Sommeria, J., 2002, "Internal Gravity Waves: From Instabilities to Turbulence," *Annu. Rev. Fluid Mech.*, **34**(1), pp. 559–593.
- [21] Monin, A. S., and Obukhov, A. M., 1954, "Basic Laws of Turbulent Mixing in the Surface Layer of the Atmosphere," *Contrib. Geophys. Inst. Acad. Sci. USSR*, **24**, pp. 163–187.
- [22] Obukhov, A. M., 1971, "Turbulence in the Atmosphere with a Non-Uniform Temperature," *Boundary Layer Meteorol.*, **2**(1), pp. 7–29.
- [23] Ferziger, J. H., Koseff, J. R., and Monismith, S. G., 2002, "Numerical Simulation of Geophysical Turbulence," *Comput. Fluids*, **31**(4–7), pp. 557–568.
- [24] Ozmidov, R. V., 1965, "On the Turbulent Exchange in a Stably Stratified Ocean," *Atmos. Oceanic Phys.*, **1**, pp. 853–860.
- [25] Bolgiano, R., 1959, "Turbulent Spectra in a Stable Stratified Atmosphere," *J. Geophys. Res.*, **64**(12), pp. 2226–2229.
- [26] Dougherty, J. P., 1961, "The Anisotropy of Turbulence at the Meteor Level," *J. Atmos. Terr. Phys.*, **21**(2–3), pp. 210–213.
- [27] Thorpe, S. A., 1973, "Experiments on Instability and Turbulence in a Stratified Shear Flow," *J. Fluid Mech.*, **61**(04), pp. 731–751.
- [28] Thorpe, S. A., 1977, "Turbulence and Mixing in a Scottish Loch," *Philos. Trans. R. Soc. London*, **286**(1334), pp. 125–181.
- [29] Dillon, T. M., 1982, "Vertical Overturns: A Comparison of Thorpe and Ozmidov Length Scales," *J. Geophys. Res.*, **87**(C12), pp. 9601–9613.
- [30] Itsweire, E. C., Koseff, J. R., Briggs, D. A., and Ferziger, J. H., 1993, "Turbulence in Stratified Shear Flows: Implications for Interpreting Shear Induced Mixing in the Ocean," *J. Phys. Oceanogr.*, **23**(7), p. 1508.
- [31] Cimattoribus, A. A., van Haren, H., and Gostiaux, L., 2014, "Comparison of Ellison and Thorpe Scales From Eulerian Ocean Temperature Observations," *J. Geophys. Res. Oceans*, **119**(10), pp. 7047–7065.
- [32] Monin, A., 1970, "The Atmospheric Boundary Layer," *Annu. Rev. Fluid Mech.*, **2**(1), pp. 225–250.
- [33] Pope, S. B., 2000, *Turbulent Flows*, Cambridge University Press, Cambridge, UK.
- [34] Ellison, T. H., 1957, "Turbulent Transport of Heat and Momentum From an Infinite Rough Plane," *J. Fluid Mech.*, **2**(5), pp. 246–466.
- [35] Taylor, J. R., Sarkar, S., and Armenio, V., 2005, "Large Eddy Simulation of Stably Stratified Open Channel Flow," *Phys. Fluids*, **17**(11), p. 116602.
- [36] Zonta, F., Onorato, M., and Soldati, A., 2012, "Turbulence and Internal Waves in Stably-Stratified Channel Flow With Temperature-Dependent Fluid Properties," *J. Fluid Mech.*, **697**, pp. 175–203.
- [37] Oberbeck, A., 1879, "Über Die Wärmeleitung Der Flüssigkeiten Bei Berücksichtigung Der Strömungen Infolge Von Temperaturdifferenzen," *Ann. Phys. Chem.*, **243**(6), pp. 271–292.
- [38] Boussinesq, J., 1903, *Theorie Analytique De La Chaleur*, Gauthier-Villars, Paris, France.
- [39] Batchelor, G. K., 1967, *An Introduction to Fluid Dynamics*, Cambridge University Press, Cambridge, UK.
- [40] Bae, J. H., Yoo, J. Y., and Choi, H., 2005, "Direct Numerical Simulation of Turbulent Supercritical Flows With Heat Transfer," *Phys. Fluids*, **17**(10), p. 105104.
- [41] Sameen, A., Verzicco, R., and Sreenivasan, K. R., 2009, "Specific Role of Fluid Properties in Non-Boussinesq Thermal Convection at the Rayleigh Number of 2×10^8 ," *Europhys. Lett.*, **86**(1), p. 14006.
- [42] Nemati, H., Patel, A., Boersma, B. J., and Pecnik, R., 2015, "Mean Statistics of a Heated Turbulent Pipe Flow at Supercritical Pressure," *Int. J. Heat Mass Transfer*, **83**, pp. 741–752.
- [43] Zonta, F., Marchioli, C., and Soldati, A., 2012, "Modulation of Turbulence in Forced Convection by Temperature-Dependent Viscosity," *J. Fluid Mech.*, **697**, pp. 150–174.
- [44] Garg, R. P., Ferziger, J. H., Monismith, S. G., and Koseff, J. R., 2000, "Stably Stratified Turbulent Channel Flows—I: Stratification Regimes and Turbulence Suppression Mechanism," *Phys. Fluids*, **12**(10), p. 2569.
- [45] García-Villalba, M., and Álamo, J. C. D., 2011, "Turbulence Modification by Stable Stratification in Channel Flow," *Phys. Fluids*, **23**(4), p. 045104.
- [46] Bejan, A., 1984, *Convective Heat Transfer*, Wiley, New York.
- [47] Gebhart, B., Jaluria, Y., Mahajan, R. L., and Sammakia, B., 1988, *Buoyancy-Induced Flows and Transport*, Hemisphere Pub. Corp., Washington, DC.
- [48] Turner, J. S., 1973, *Buoyancy Effects in Fluids*, Cambridge University Press, Cambridge, UK.
- [49] Spiegel, E. A., and Veronis, G., 1960, "On the Boussinesq Approximation for a Compressible Fluid," *Astrophys. J.*, **131**, pp. 442–447.
- [50] Mihaljan, J. M., 1962, "A Rigorous Exposition of the Boussinesq Approximations Applicable to a Thin Layer of Fluid," *Astrophys. J.*, **136**, pp. 1126–1133.
- [51] Gray, D. D., and Giorgini, A., 1976, "The Validity of the Boussinesq Approximation for Liquids and Gases," *Int. J. Heat Mass Transfer*, **19**(5), pp. 545–551.
- [52] Niemela, J. J., 2004, "High Rayleigh Number Thermal Convection," *J. Low Temp. Phys.*, **134**(1/2), pp. 447–456.
- [53] Niemela, J. J., and Sreenivasan, K., 2006, "The Use of Cryogenic Helium for Classical Turbulence: Promises and Hurdles," *J. Low Temp. Phys.*, **143**(5–6), pp. 163–212.
- [54] Kundu, P. K., Cohen, I. M., and Dowling, D. R., 2011, *Fluid Mechanics*, 5th ed., Academic Press, Waltham, MA.
- [55] Tritton, D. J., 1988, *Physical Fluid Dynamics*, Oxford University Press, Oxford, UK.
- [56] Pons, M., and Quéré, P. L., 2007, "Modeling Natural Convection With the Work of Pressure-Forces: A Thermodynamic Necessity," *Int. J. Numer. Methods Fluids*, **13**(3), pp. 322–332.
- [57] Ogura, Y., and Phillips, N., 1962, "Scale Analysis of Deep and Shallow Convection in the Atmosphere," *J. Atmos. Sci.*, **19**(2), pp. 173–179.
- [58] Bannon, P. R., 1996, "On the Anelastic Approximation for a Compressible Atmosphere," *J. Atmos. Sci.*, **53**(23), pp. 3618–3628.
- [59] Lilly, D. K., 1996, "A Comparison of Incompressible, Anelastic and Boussinesq Dynamics," *Atmos. Res.*, **40**(2–4), pp. 143–151.
- [60] Sugiyama, K., Calzavarini, E., Grossmann, S., and Lohse, D., 2009, "Flow Organization in Two-Dimensional Non-Oberbeck-Boussinesq Rayleigh-Benard Convection in Water," *J. Fluid Mech.*, **637**, pp. 105–135.
- [61] Zonta, F., and Soldati, A., 2014, "Effect of Temperature-Dependent Fluid Properties on Heat Transfer in Turbulent Mixed Convection," *ASME J. Heat Transfer*, **136**(2), p. 022501.
- [62] Pickard, G. L., and Emery, W. J., 1990, *Descriptive Physical Oceanography: An Introduction*, Pergamon Press, Oxford, UK.
- [63] Agostini, B., Fabbri, M., Park, J. E., Wojtan, L., Thome, J. R., and Michel, B., 2007, "State of the Art of High Heat Flux Cooling Technologies," *Heat Transfer Eng.*, **28**(4), pp. 258–281.
- [64] Moin, P., and Mahesh, K., 1998, "Direct Numerical Simulation: A Tool in Turbulence Research," *Annu. Rev. Fluid Mech.*, **30**(1), pp. 539–578.
- [65] Lesieur, M., and Métais, O., 1996, "New Trends in Large-Eddy Simulations of Turbulence," *Annu. Rev. Fluid Mech.*, **28**(1), pp. 45–82.
- [66] Durbin, P. A., 2018, "Some Recent Developments in Turbulence Closure Modeling," *Annu. Rev. Fluid Mech.*, **50**(1), pp. 77–103.
- [67] Miles, J. W., 1961, "On the Stability of Heterogeneous Shear Flows," *J. Fluid Mech.*, **10**(04), pp. 496–508.
- [68] Gage, K. S., and Reid, W. H., 1968, "The Stability of Thermally Stratified Plane Poiseuille Flow," *J. Fluid Mech.*, **33**(01), pp. 21–32.
- [69] Deusebio, E., Caulfield, C. P., and Taylor, J. R., 2015, "The Intermittency Boundary in Stratified Plane Couette Flow," *J. Fluid Mech.*, **781**, pp. 298–329.
- [70] Brethouwer, G., Duguet, Y., and Schlatter, P., 2012, "Turbulent-Laminar Coexistence in Wall Flows With Coriolis, Buoyancy or Lorentz Forces," *J. Fluid Mech.*, **704**, pp. 137–172.
- [71] He, P., 2016, "A High Order Finite Difference Solver for Massively Parallel Simulations of Stably Stratified Turbulent Channel Flows," *Comput. Fluids*, **127**, pp. 161–173.
- [72] de Wiel, B. J. H. V., Moene, A. F., Jonker, H. J. J., and Holtslag, A. A. M., 2012, "The Cessation of Continuous Turbulence as Precursor of the Very Stable Nocturnal Boundary Layer," *J. Atmos. Sci.*, **69**(11), pp. 3097–3115.
- [73] Donda, J. M. M., van Hooijdonk, I. G. S., Moene, A. F., Jonker, H. J. J., van Heijst, G. J. F., Clercx, H. J. H., and van de Wiel, B. J. H., 2015, "Collapse of Turbulence in Stably Stratified Channel Flow: A Transient Phenomenon," *Quart. J. Roy. Meteor. Soc.*, **141** (691), pp. 2137–2147.
- [74] Monin, A. S., and Yaglom, A. M., 1975, *Statistical Fluid Mechanics: Mechanism of Turbulence*, Vol. 2, MIT Press, Cambridge, MA.
- [75] Iida, O., Kasagi, N., and Nagano, Y., 2002, "Direct Numerical Simulation of Turbulent Channel Flow Under Stable Density Stratification," *Int. J. Heat Mass Transfer*, **45**(8), pp. 1693–1703.
- [76] Yeo, K., Kim, B. G., and Lee, C., 2009, "Eulerian and Lagrangian Statistics in Stably Stratified Turbulent Channel Flows," *J. Turbul.*, **10**, pp. 1–26.
- [77] Flores, O., and Riley, J. J., 2011, "Analysis of Turbulence Collapse in the Stably Stratified Surface Layer Using Direct Numerical Simulation," *Boundary Layer Meteorol.*, **139**(2), pp. 241–159.
- [78] Deusebio, E., Schlatter, P., Brethouwer, G., and Lindborg, E., 2011, "Direct Numerical Simulations of Stratified Open Channel Flows," *J. Phys. Conf. Ser.*, **318**, pp. 241–259.
- [79] Lovecchio, S., Zonta, F., and Soldati, A., 2014, "Influence of Thermal Stratification on the Surfacing and Clustering of Floaters in Free Surface Turbulence," *Adv. Water Resour.*, **72**, pp. 22–31.

- [80] Coleman, G. N., Ferziger, J. H., and Spalart, P. R., 1992, "Direct Numerical Simulation of the Stably Stratified Turbulent Ekman Layer," *J. Fluid Mech.*, **244**(1), pp. 677–712.
- [81] Lovecchio, S., Zonta, F., and Soldati, A., 2015, "Upscale Energy Transfer and Flow Topology in Free Surface Turbulence," *Phys. Rev. E Stat. Nonlin. Soft. Matter. Phys.*, **91**(3), p. 033010.
- [82] Basak, S., and Sarkar, S., 2006, "Dynamics of a Stratified Shear Layer With Horizontal Shear," *J. Fluid Mech.*, **568**, pp. 19–54.
- [83] Jacobitz, F. G., Sarkar, S., and van Atta, C. W., 1997, "Direct Numerical Simulations of the Turbulence Evolution in a Uniformly Sheared and Stratified Flow," *J. Fluid Mech.*, **342**, pp. 231–261.
- [84] Brost, R. A., and Wyngaard, J. C., 1978, "A Model Study of the Stably-Stratified Planetary Boundary Layer," *J. Atmos. Sci.*, **35**(8), pp. 1427–1440.
- [85] Hunt, J. C. R., 1985, "Diffusion in the Stably Stratified Atmospheric Boundary Layer," *J. Clim. Appl. Meteorol.*, **24**(11), pp. 1187–1195.
- [86] Nieuwstadt, F. T. M., 1984, "The Turbulent Structure of the Stable, Nocturnal Boundary Layer," *J. Atmos. Sci.*, **41**(14), pp. 2202–2216.
- [87] Caughey, S. J., Wyngaard, J. C., and Kaimal, J. C., 1979, "Turbulence in the Evolving Stable Boundary Layer," *J. Atmos. Sci.*, **6**, pp. 1041–1052.
- [88] Mason, P. J., and Derbyshire, S. H., 1990, "Large-Eddy Simulation of the Stably-Stratified Atmospheric Boundary Layer," *Boundary Layer Meteorol.*, **53**(1–2), pp. 117–162.
- [89] Derbyshire, S. H., 1995, "Stable Boundary Layers: Observations, Models and Variability—Part I: Modelling and Measurements," *Boundary Layer Meteorol.*, **74**(1–2), pp. 19–54.
- [90] Saiki, E. S., Moeng, C. H., and Sullivan, P. P., 2000, "Large-Eddy Simulation of the Stably Stratified Planetary Boundary Layer," *Boundary Layer Meteorol.*, **95**(1), pp. 1–30.
- [91] Kosovic, B., and Curry, J. A., 2000, "A Large Eddy Simulation Study of a Quasi-Steady Stably Stratified Atmospheric Boundary Layer," *J. Atmos. Sci.*, **57**(8), pp. 1052–1068.
- [92] Beare, R. J., MacVean, M. K., Holtslag, A. A. M., Cuxart, J., Esau, I., Golaz, J.-C., Jimenez, M. A., Khairoutdinov, M., Kosovic, B., Lewellen, D., Lund, T. S., Lundquist, J. K., McCabe, A., Moene, A. F., Noh, Y., Raasch, S., and Sullivan, P., 2006, "An Intercomparison of Large-Eddy Simulations of the Stable Boundary Layer," *Boundary Layer Meteorol.*, **118**(2), pp. 247–272.
- [93] Kleissl, J., Vijayant, K., and Parlange, C. M. M. B., 2006, "Numerical Study of Dynamic Smagorinsky Models in Large-Eddy Simulation of the Atmospheric Boundary Layer: Validation in Stable and Unstable Conditions," *Water Resour. Res.*, **42**(6), p. W06D10.
- [94] Germano, M., Piomelli, U. M. M. P., and Cabot, W. H., 1991, "A Dynamic Subgrid-Scale Eddy Viscosity Model," *Phys. Fluids A*, **3**, pp. 1760–1765.
- [95] Porté-Agel, F., 2004, "A Scale-Dependent Dynamic Model for Scalar Transport in Large-Eddy Simulations of the Atmospheric Boundary Layer," *Boundary Layer Meteorol.*, **112**(1), pp. 81–105.
- [96] Stoll, R., and Porté-Agel, F., 2008, "Large-Eddy Simulation of the Stable Atmospheric Boundary Layer Using Dynamic Models With Different Averaging Schemes," *Boundary Layer Meteorol.*, **126**(1), pp. 1–28.
- [97] Wang, L., and Lu, X. Y., 2005, "Large Eddy Simulation of Stably Stratified Turbulent Open Channel Flows With Low-to-High-Prandtl Number," *Int. J. Heat Mass Transfer*, **48**(10), pp. 1883–1897.
- [98] Jiménez, M. A., and Cuxart, J., 2005, "Large-Eddy Simulations of the Stable Boundary Layer Using the Standard Kolmogorov Theory: Range of Applicability," *Boundary Layer Meteorol.*, **115**(2), pp. 241–261.
- [99] Cuxart, J., Yagüe, C., Morales, G., Terradellas, E., Orbe, J., Calvo, J., Fernandez, A., Infante, C., Buenestado, P., Espinalt, A., Jorgensen, H., Rees, J., Vila, J., Redondo, J., Cantalapiebra, L., and Conangla, L., 2000, "Stable Atmospheric Boundary-Layer Experiment in Spain (Sables 98): A Report," *Boundary Layer Meteorol.*, **96**(3), pp. 19–54.
- [100] Poulos, G. S., Blumen, W., Fritts, D. C., Lundquist, J. K., Sun, J., Burns, S. P., Nappo, C., Cuxart, R. B. R. N. J., Terradellas, E., Balsley, B., and Jensen, M., 2002, "Cases-99: A Comprehensive Investigation of the Stable Nocturnal Boundary Layer," *Bull. Am. Meteorol. Soc.*, **83**(4), pp. 555–581.
- [101] Jones, W. P., and Launder, B. R., 1972, "The Prediction of Laminarization With a Two-Equation Model of Turbulence," *Int. J. Heat Mass Transfer*, **15**(2), pp. 301–314.
- [102] Munk, W. H., and Anderson, E. R., 1948, "Notes on the Theory of the Thermocline," *J. Mar. Res.*, **3**, pp. 276–295.
- [103] Schumann, U., and Gerz, T., 1995, "Turbulent Mixing in Stably Stratified Shear Flows," *J. Appl. Meteorol.*, **34**(1), pp. 33–48.
- [104] Venayagamoorthy, S. K., and Stretch, D. D., 2010, "On the Turbulent Prandtl Number in Homogeneous Stably Stratified Turbulence," *J. Fluid Mech.*, **644**, pp. 359–369.
- [105] Garratt, J. R., 1992, *The Atmospheric Boundary Layer*, Cambridge University Press, Cambridge, UK.
- [106] Derbyshire, S. H., 1999, "Stable Boundary-Layer Modelling: Established Approaches and Beyond," *Boundary Layer Meteorol.*, **90**(3), pp. 423–446.
- [107] Huang, J., Bou-Zeid, E., and Golaz, J.-C., 2013, "Turbulence and Vertical Fluxes in the Stable Atmospheric Boundary Layer—Part II: A Novel Mixing-Length Model," *J. Atmos. Sci.*, **70**(6), pp. 1528–1542.
- [108] Fernando, H. J. S., and Weil, J. C., 2010, "Whither the Stable Boundary Layer?," *Bull. Am. Meteorol. Soc.*, **91**(11), pp. 1475–1484.
- [109] Mahrt, L., and Vickers, D., 2005, "Boundary-Layer Adjustment Over Small-Scale Changes of Surface Heat Flux," *Boundary Layer Meteorol.*, **116**(2), pp. 313–330.
- [110] Galperin, B., Sukoriansky, S., and Anderson, P. S., 2007, "On the Critical Richardson Number in Stably Stratified Turbulence," *Atmos. Sci. Lett.*, **8**(3), pp. 65–69.
- [111] Zilitinkevich, S., Elperin, T., Kleerorin, N., Rogachevskii, I., Esau, I., Mauritsen, T., and Miles, M., 2008, "Turbulence Energetics in Stably Stratified Geophysical Flows: Strong and Weak Mixing Regimes," *Quart. J. R. Meteorol. Soc.*, **134**(633), pp. 793–799.
- [112] Karimpour, F., and Venayagamoorthy, S. K., 2014, "A Simple Turbulence Model for Stably Stratified Wall-Bounded Flows," *J. Geophys. Res.*, **119**(2), pp. 870–880.
- [113] Mellor, G. L., and Yamada, T., 1974, "A Hierarchy of Turbulence Closure Models for Planetary Boundary Layers," *J. Atmos. Sci.*, **31**(7), pp. 1791–1806.
- [114] Canuto, V. M., Cheng, Y., Howard, A., and Isau, I., 2008, "Stably Stratified Flows: A Model With No Ri(Cr)," *J. Atmos. Sci.*, **65**(7), pp. 2437–2447.
- [115] Lazeroms, W. M. J., Brethouwer, G., Wallin, S., and Johansson, A. V., 2013, "An Explicit Algebraic Reynolds-Stress and Scalar-Flux Model for Stably Stratified Flows," *J. Fluid Mech.*, **723**, pp. 91–125.
- [116] Zonta, F., 2013, "Nusselt Number and Friction Factor in Thermally Stratified Turbulent Channel Flow Under Non-Oberbeck–Boussinesq Conditions," *Int. J. Heat Fluid Flow*, **44**, pp. 489–494.
- [117] Piccirillo, P., and van Atta, C. W., 1997, "The Evolution of a Uniformly Sheared Thermally Stratified Turbulent Flow," *J. Fluid Mech.*, **334**, pp. 61–86.
- [118] Arya, S. P. S., 1975, "Buoyancy Effects in a Horizontal Flat-Plane Boundary Layer," *J. Fluid Mech.*, **68**(02), pp. 321–343.
- [119] Komori, S., Ueda, H., Ogino, F., and Mizushima, T., 1983, "Turbulence Structure in Stably Stratified Open-Channel Flow," *J. Fluid Mech.*, **130**(1), pp. 13–26.
- [120] Webster, C. A. G., 1964, "An Experimental Study of Turbulence in a Density Stratified Shear Flow," *J. Fluid Mech.*, **19**(02), pp. 221–245.
- [121] Piat, J.-F., and Hopfinger, E. J., 1981, "A Boundary Layer Topped by a Density Interface," *J. Fluid Mech.*, **113**(1), pp. 411–432.
- [122] Ohya, Y., Neff, D., and Meroney, R., 1997, "Turbulence Structure in a Stratified Boundary Layer Under Stable Conditions," *Boundary Layer Meteorol.*, **83**(1), pp. 139–161.
- [123] Ohya, Y., and Uchida, T., 2003, "Turbulence Structure of Stable Boundary Layers With a Near-Linear Temperature Profile," *Boundary Layer Meteorol.*, **108**(1), pp. 19–38.
- [124] Ohya, Y., 2001, "Wind Tunnel Study of Atmospheric Stable Boundary Layers Over a Rough Surface," *Boundary Layer Meteorol.*, **98**(1), pp. 57–82.
- [125] Ivey, G. N., Winters, K. B., and Koseoff, J. R., 2008, "Density Stratification, Turbulence, But How Much Mixing?," *Annu. Rev. Fluid Mech.*, **40**(1), pp. 169–184.
- [126] Cimattoribus, A. A., and van Haren, H., 2015, "Temperature Statistics Above a Deep-Ocean Sloping Boundary," *J. Fluid Mech.*, **775**, pp. 415–435.
- [127] Riley, J. J., and Lindborg, E., 2008, "Stratified Turbulence: A Possible Interpretation of Some Geophysical Turbulence Measurements," *J. Atmos. Sci.*, **65**(7), pp. 2416–2424.
- [128] Itsweire, E., 1984, "Measurements of Vertical Overturns in a Stably Stratified Turbulent Flow," *Phys. Fluids*, **27**(4), pp. 764–766.
- [129] Ledwell, J. R., Watson, A. J., and Law, C. S., 1998, "Mixing of a Tracer in the Pycnocline," *J. Geophys. Res.*, **103**(C10), pp. 21499–21529.
- [130] Ledwell, J. R., Montgomery, E. T., Polzin, K. L., Laurent, L. C. S., Schmitt, R. W., and Toole, J. M., 2000, "Evidence for Enhanced Mixing Over Rough Topography in the Abyssal Ocean," *Nature*, **403**(6766), pp. 79–182.
- [131] Lueck, R. G., Wolk, F., and Yamazaki, H., 2002, "Oceanic Velocity Microstructure Measurements in the 20th Century," *J. Oceanogr.*, **58**(1), pp. 153–174.
- [132] Álamo, J. C. D., and Jiménez, J., 2003, "Spectra of the Very Large Anisotropic Scales in Turbulent Channels," *Phys. Fluids*, **15**(6), p. L41.
- [133] Hoyas, S., and Jiménez, J., 2006, "Scaling of the Velocity Fluctuations in Turbulent Channels Up to $Re_\tau = 2003$," *Phys. Fluids*, **18**(1), p. 011702.
- [134] Lighthill, M. J., 1978, *Waves in Fluids*, Cambridge University Press, Cambridge, UK.
- [135] Pomar, L., Morsilli, M., Hallock, P., and Bádenas, B., 2012, "Internal Waves, an Under-Explored Source of Turbulence Events in the Sedimentary Record," *Earth Sci. Rev.*, **11**(1–2), pp. 56–81.
- [136] Lamb, K. G., 2014, "Internal Wave Breaking and Dissipation Mechanisms on the Continental Slope/Shelf," *Annu. Rev. Fluid Mech.*, **46**(1), pp. 231–254.
- [137] Peltier, W. R., and Caulfield, C. P., 2003, "Mixing Efficiency in Stratified Shear Flows," *Annu. Rev. Fluid Mech.*, **35**(1), pp. 135–167.
- [138] Sun, J., 1999, "Diurnal Variations of Thermal Roughness Height Over a Grassland," *Boundary Layer Meteorol.*, **92**(3), pp. 407–427.
- [139] Mahrt, L., 1998, "Stratified Atmospheric Boundary Layers and Breakdown of Models," *J. Theor. Comput. Fluid Dyn.*, **11**(3–4), pp. 263–279.
- [140] Hogstrom, U., 1996, "Review of Some Basic Characteristics of the Atmospheric Surface Layer," *Bound. Layer Meteorol.*, **78**, pp. 215–246.
- [141] de Wiel, B. J. H. V., Moene, A. F., Hartogensis, O. K., Bruin, H. A. R. D., and Holtslag, A. A. M., 2003, "Intermittent Turbulence in the Stable Boundary Layer Over Land—Part II: A Classification for Observations During Cases-99," *J. Atmos. Sci.*, **60**(20), pp. 2509–2522.
- [142] Fukui, K., Nakajima, M., and Ueda, H., 1983, "A Laboratory Experiment on Momentum and Heat Transfer in the Stratified Surface Layer," *Quart. J. R. Met. Soc.*, **109**(461), pp. 661–676.
- [143] Lessani, B., and Zainali, A., 2009, "Numerical Investigation of Stably Stratified Turbulent Channel Flow Under Non-Boussinesq Conditions," *J. Turbul.*, **10**, pp. 1–25.

- [144] Bae, J. H., Yoo, J. Y., and McEligot, D. M., 2008, "Direct Numerical Simulation of Heated CO_2 Flows at Supercritical Pressure in a Vertical Annulus at $\text{Re} = 8900$," *Phys. Fluids*, **20**(5), p. 055108.
- [145] Hamilton, J., Kim, J., and Waleffe, F., 1995, "Regeneration Mechanisms of Near-Wall Turbulence Structures," *J. Fluid Mech.*, **287**(1), pp. 317–348.
- [146] Waleffe, F., 1997, "On a Self-Sustaining Process in Shear Flows," *Phys. Fluids*, **9** (4), pp. 883–900.
- [147] Peeters, J. W. R., Pecnik, R., Rohde, M., van der Hagen, T. H. J. J., and Boersma, B. J., 2016, "Turbulence Attenuation in Simultaneously Heated and Cooled Annular Flows at Supercritical Pressure," *J. Fluid Mech.*, **799**, pp. 505–540.
- [148] Patel, A., Boersma, B., and Pecnik, R., 2016, "The Influence of Near-Wall Density and Viscosity Gradients on Turbulence in Channel Flows," *J. Fluid Mech.*, **809**, pp. 793–820.
- [149] Paparella, F., and Hardenberg, J. V., 2012, "Clustering of Salt Fingers in Double-Diffusive Convection Leads to Staircaselike Stratification," *Phys. Rev. Lett.*, **109**(1), p. 014502.
- [150] Yang, Y., Verzicco, R., and Lohse, D., 2016, "Scaling Laws and Flow Structures of Double Diffusive Convection in the Finger Regime," *J. Fluid Mech.*, **802**, pp. 667–689.
- [151] Taylor, J. R., and Sarkar, S., 2008, "Direct and Large Eddy Simulations of a Bottom Ekman Layer Under an External Stratification," *Int. J. Heat Fluid Flow*, **29**(3), pp. 721–732.
- [152] Deusebio, E., Brethouwer, G., Schlatter, P., and Lindborg, E., 2014, "A Numerical Study of the Unstratified and Stratified Ekman Layer," *J. Fluid Mech.*, **755**, pp. 672–704.
- [153] Anson, C., and Mellado, J. P., 2014, "Global Intermittency and Collapsing Turbulence in the Stratified Planetary Boundary Layer," *Boundary Layer Meteorol.*, **153**(1), pp. 89–116.